

CONTRACTOR REPORT

SAND91-7071
Unlimited Release
UC-721



SAND91-7071
0002
UNCLASSIFIED

07/92
74P STAC

Consolidation of the Waste Isolation Pilot Plant Crushed Salt/Bentonite Mixtures as a Function of Confining Pressure and Moisture Content as Compared With Constitutive Model Predictions

Nancy S. Brodsky, Tom W. Pfeifle
RE/SPEC Inc.
PO Box 725
Rapid City, SD 57709

Prepared by Sandia National Laboratories Albuquerque, New Mexico 87185
and Livermore, California 94550 for the United States Department of Energy
under Contract DE-AC04-76DP00789

Printed July 1992

Issued by Sandia National Laboratories, operated for the United States Department of Energy by Sandia Corporation.

NOTICE: This report was prepared as an account of work sponsored by an agency of the United States Government. Neither the United States Government nor any agency thereof, nor any of their employees, nor any of their contractors, subcontractors, or their employees, makes any warranty, express or implied, or assumes any legal liability or responsibility for the accuracy, completeness, or usefulness of any information, apparatus, product, or process disclosed, or represents that its use would not infringe privately owned rights. Reference herein to any specific commercial product, process, or service by trade name, trademark, manufacturer, or otherwise, does not necessarily constitute or imply its endorsement, recommendation, or favoring by the United States Government, any agency thereof or any of their contractors or subcontractors. The views and opinions expressed herein do not necessarily state or reflect those of the United States Government, any agency thereof or any of their contractors.

Printed in the United States of America. This report has been reproduced directly from the best available copy.

Available to DOE and DOE contractors from
Office of Scientific and Technical Information
PO Box 62
Oak Ridge, TN 37831

Prices available from (615) 576-8401, FTS 626-8401

Available to the public from
National Technical Information Service
US Department of Commerce
5285 Port Royal Rd
Springfield, VA 22161

NTIS price codes
Printed copy: A04
Microfiche copy: A01

Consolidation of the Waste Isolation Pilot Plant Crushed Salt/Bentonite Mixtures as a Function of Confining Pressure and Moisture Content as Compared With Constitutive Model Predictions¹

Nancy S. Brodsky and Tom W. Pfeifle
RE/SPEC Inc.
P.O. Box 725
Rapid City, SD 57709

ABSTRACT

Four hydrostatic consolidation tests were performed on crushed salt/bentonite mixtures to evaluate the influence of moisture on consolidation rate, permeability, and compressive strength. Specimens comprised 30 percent bentonite and 70 percent salt based on total dry weight. Brine was added to each specimen to adjust its total moisture content to between 3.5 and 10 percent (nominal) of the total dry weight. In the consolidation tests, each specimen was subjected to two stages of hydrostatic stress: 0.5 MPa and 3.45 MPa. During each stage, the pressure was maintained at a constant level and volumetric strain data were continuously logged. By using multiple stages, consolidation data were obtained at two pressures and the time required to consolidate the specimens to full saturation was reduced. Once full saturation was achieved, specimens were subjected to a final test stage in which the hydrostatic stress was reduced and a permeability test was performed. A steady flow permeability test was performed successfully on only one specimen and its permeability was determined to be $1.12 \times 10^{-19} \text{ m}^2$. An unconfined compressive strength test was conducted on one of the consolidated specimens and was found to be 1.66 MPa.

A density model proposed by Sjaardema and Krieg was compared to the dry density data using parameter values established by Callahan and DeVries. The model fit the data best at intermediate moisture contents and low pressures. The model was also fitted to the data obtained in this study to determine additional parameter values.

¹The content of this report was effective as of September 1991. This report was prepared by RE/SPEC Inc. under Contract 69-1730 with Sandia National Laboratories.

TABLE OF CONTENTS

1.0 INTRODUCTION	1
1.1 BACKGROUND	1
1.2 APPROACH AND SCOPE	1
1.3 REPORT ORGANIZATION	2
2.0 SPECIMENS	5
2.1 MATERIALS	5
2.2 PREPARATION	6
2.2.1 Sample	6
2.2.2 Specimen	6
2.3 POST-TEST DISPOSITION	8
3.0 TEST APPARATUS	9
3.1 CONSOLIDATION	9
3.1.1 Load Frame	9
3.1.2 Instrumentation	9
3.1.3 Control	11
3.2 PERMEABILITY	11
3.3 STRENGTH	11
3.3.1 Load Frame	11
3.3.2 Instrumentation and Control	14
3.4 CALIBRATION	14
4.0 TEST PROCEDURES	17
4.1 DENSITY	17
4.2 CONDITIONING	17
4.3 CONSOLIDATION	18
4.4 PERMEABILITY	19
4.5 STRENGTH	20
4.6 WATER DISTRIBUTION	21

TABLE OF CONTENTS
(CONTINUED)

5.0 TEST RESULTS	23
5.1 CONSOLIDATION	23
5.1.1 Volumetric Strain	23
5.1.2 Density	28
5.2 PERMEABILITY	34
5.3 STRENGTH	34
5.4 WATER CONTENT DISTRIBUTION	36
6.0 MODEL FITTING	41
7.0 SUMMARY AND CONCLUSIONS	55
8.0 REFERENCES	57

LIST OF TABLES

1-1	Consolidation Test Conditions	3
2-1	Specimen Identification Numbers	8
3-1	Transducer Ranges and Resolutions	15
4-1	Densities Before and After Conditioning	19
5-1	Summary of Density Data for Creep Consolidation Tests	29
5-2	Summary of Permeabilities and Strength	36
5-3	Water Content Distribution for Test CS5	39
6-1	Parameter Values for Density Model	43

LIST OF FIGURES

2-1	Specimen assembly.	7
3-1	Testing frame for consolidation tests.	10
3-2	Schematic of brine permeability test system.	12
3-3	Test frame for constant strain-rate tests.	13
5-1	Volumetric strain-versus-time for WIPP-CS5, 70/30 crushed salt/bentonite.	24
5-2	Volumetric strain-versus-time for WIPP-CS6, 70/30 crushed salt/bentonite.	25
5-3	Volumetric strain-versus-time for WIPP-CS7, 70/30 crushed salt/bentonite.	26
5-4	Volumetric strain-versus-time for WIPP-CS8, 70/30 crushed salt/bentonite.	27
5-5	Wet and dry density as a function of time for WIPP-CS5, 70/30 crushed salt/bentonite.	30
5-6	Wet and dry density as a function of time for WIPP-CS6, 70/30 crushed salt/bentonite.	31
5-7	Wet and dry density as a function of time for WIPP-CS7, 70/30 crushed salt/bentonite.	32
5-8	Wet and dry density as a function of time for WIPP-CS8, 70/30 crushed salt/bentonite.	33
5-9	Brine flow as a function of time for WIPP-CS6.	35
5-10	Stress-strain curve for unconfined compressive strength test of WIPP-CS5, 70/30 crushed salt/bentonite.	37
5-11	Unconfined compressive strength as a function of density for consolidated specimens of WIPP 70/30 crushed salt/bentonite.	38
6-1	Log ₁₀ volumetric strain rate-versus-fractional density for WIPP-CS5, 70/30 crushed salt/bentonite, and prediction based on Sjaardema and Krieg [1987] constitutive model with parameters fit by Callahan and DeVries [1991].	44

LIST OF FIGURES (CONTINUED)

6-2	Log_{10} volumetric strain rate-versus-fractional density for WIPP-CS6, 70/30 crushed salt/bentonite, and prediction based on Sjaardema and Krieg [1987] constitutive model with parameters fit by Callahan and DeVries[1991].	45
6-3	Log_{10} volumetric strain rate-versus-fractional density for WIPP-CS7, 70/30 crushed salt/bentonite, and prediction based on Sjaardema and Krieg [1987] constitutive model with parameters fit by Callahan and DeVries [1991].	46
6-4	Log_{10} volumetric strain rate-versus-fractional density for WIPP-CS8, 70/30 crushed salt/bentonite, and prediction based on Sjaardema and Krieg [1987] constitutive model with parameters fit by Callahan and DeVries [1991].	47
6-5	A comparison of three sets of parameter values used in the Sjaardema and Krieg [1987] constitutive model at 0.05 MPa pressure.	48
6-6	A comparison of three sets of parameter values used in the Sjaardema and Krieg [1987] constitutive model at 15 MPa pressure.	49
6-7	Log_{10} volumetric strain rate-versus-fractional density for WIPP-CS5, 70/30 crushed salt/bentonite and prediction based on Sjaardema and Krieg [1987] constitutive model with parameters fit in this study. . .	50
6-8	Log_{10} volumetric strain rate-versus-fractional density for WIPP-CS6, 70/30 crushed salt/bentonite and prediction based on Sjaardema and Krieg [1987] constitutive model with parameters fit in this study. . .	51
6-9	Log_{10} volumetric strain rate-versus-fractional density for WIPP-CS7, 70/30 crushed salt/bentonite and prediction based on Sjaardema and Krieg [1987] constitutive model with parameters fit in this study. . .	52
6-10	Log_{10} volumetric strain rate-versus-fractional density for WIPP-CS8, 70/30 crushed salt/bentonite and prediction based on Sjaardema and Krieg [1987] constitutive model with parameters fit in this study. . .	53

1.0 INTRODUCTION

1.1 BACKGROUND

Crushed salt, mixed with bentonite to reduce permeability and to absorb radionuclides, is a primary candidate backfill material considered for use in the Waste Isolation Pilot Plant (WIPP) storage and access rooms. Crushed salt will be produced in large volumes during mining of the access and storage rooms and is compatible with the host rock. The permeability of the backfill is important because transport of soluble radionuclides by brine flow is of primary interest in determining the performance of the repository. Backfill permeability will likely decrease with time as the backfill consolidates under the load produced by deformation of the surrounding intact host rock, as pore space is reduced and isolated, and as surface grain contacts are strengthened. Therefore, the mechanics of backfill consolidation and the variables that influence consolidation are of interest because of their expected relationship to permeability.

1.2 APPROACH AND SCOPE

Four consolidation tests were conducted under hydrostatic stresses between 0.5 and 3.45 MPa and at a temperature of 25°C using apparatus and specimens similar to those used by Holcomb and Hannum [1982], Pfeifle and Senseny [1985], Stroup and Senseny [1987], and Pfeifle [1991] to evaluate the influence of moisture on consolidation rate, permeability, and compressive strength of crushed salt/bentonite backfill. This work is an extension of work done by Pfeifle [1991] in which three consolidation tests were performed on salt/bentonite mixtures at different moisture contents and pressures.

The specimens were prepared from batch samples of 70 percent crushed salt and 30 percent bentonite by dry weight. Brine was added to the batch samples to adjust the nominal water content to 3.5, 7, or 10 percent of the total dry weight (i.e., the total weight of the specimen minus the weight of water). The equivalent nominal water content based on the total specimen weight (i.e., the weight of crushed salt, bentonite, and water) was then either 3.4, 6.5, or 9.1 percent, respectively. The specimen volume was determined using a fluid displacement technique and density was determined from the specimen mass and volume.

The conditions imposed during the tests were selected by Sandia National Laboratories Experimental Division, Albuquerque, New Mexico, as the tests proceeded. The objectives of the tests were (1) to measure the time-dependent consolidation of specimens at selected water contents and compare these data with predicted consolidation rates; (2) to determine permeability of each specimen using the steady flow of brine technique once saturation was achieved; and (3) to measure the strength of each consolidated specimen. To achieve these objectives, multiple stages of

successively higher pressures were imposed during each test to acquire volumetric strain-time data at several pressures and also to reduce the overall time required to reach saturation by accelerating the rate of consolidation. Volumetric strain was measured continuously during the consolidation phase of the tests to provide a complete history of consolidation. Table 1-1 lists the prescribed conditions for each consolidation stage of the four tests. Full saturation was achieved in three of the four specimens. These three specimens were subjected to a final stage in which the hydrostatic stress was reduced and a permeability test was initiated; however, a successful permeability measurement was completed for only one test (CS6). After the final stage, the unconfined compressive strength of one specimen (CS5) was determined by loading it at a constant strain rate of $10^{-5} \cdot \text{s}^{-1}$. The water content profile parallel to the specimen axis was then determined for this specimen by sectioning it at eight locations normal to its axis and performing water content determinations on the samples obtained.

1.3 REPORT ORGANIZATION

In addition to this introduction, this report has seven chapters. Chapter 2 describes the specimens and Chapter 3 describes the testing apparatus. Chapter 4 gives the test procedures and is followed by Chapter 5, which gives the test results. In Chapter 6, the experimental data are compared with predicted values based on a constitutive model. Chapter 7 contains a summary and the conclusions of the study and is followed by Chapter 8, a list of cited references.

Table 1-1. Consolidation Test Conditions

Test No.	Water ^(a) Content		Stage	Hydrostatic Stress (MPa)
	Dry Wt. ^(b) (%)	Total Wt. ^(c) (%)		
1 (CS5)	7.47	6.95	1	0.5
			2	3.45
			3	0.5 ^(d)
2 (CS6)	10.85	9.79	1	0.5
			2	3.45
			3	0.5 ^(d)
3 (CS7)	3.38	3.27	1	0.5
			2	3.45
4 (CS8)	7.46	6.94	1	0.5
			2	3.45
			3	0.5 ^(d)

(a) These are measured water contents; the amount of brine added to each specimen was adjusted to account for the moisture of the salt and bentonite and for the dissolved solids in the brine.

(b) Defined as the ratio (expressed as a percentage) of the weight (mass) of water in a given material to the weight (mass) of solid material particles.

(c) Defined as the ratio (expressed as a percentage) of the weight (mass) of water in a given material to the total weight (mass) of all materials including liquids and solids.

(d) Permeability test.

2.0 SPECIMENS

2.1 MATERIALS

Two materials were combined to produce batch samples that were then used to prepare the individual test specimens. The samples were 70 percent crushed salt and 30 percent bentonite by dry weight. After the materials were mixed, saturated brine was added to the samples to produce nominal water contents ranging from approximately 3.5 to 10 percent of the total dry sample weight, or 3.4 to 9.1 percent of the total sample weight (i.e., crushed salt, bentonite, and water).

The crushed salt used in the samples was provided by Sandia National Laboratories and was produced by a continuous miner during development of the WIPP test facility. The mine-run salt contains particles that range in size up to several centimeters. Because the test specimens have a nominal diameter of only 102 mm, the mine-run salt was sieved to remove particles larger than 9.5 mm to produce a specimen-diameter-to-maximum-particle-size ratio of about 10. The water content of the crushed salt was 0.23 percent by dry weight as determined from three samples that ranged in mass from 151 g to 214 g dried for 7 days at 110°C. Moisture content was determined by drying each sample until its weight was constant to within 0.1 percent over a period of 1 day. This water content does not represent the as-mined water content because no special measures were taken to preserve the water content either in shipping or during storage. Published values for the density of salt solids range from 1,900 to 2,200 kg·m⁻³. For this study, the assumed solid density of the salt was 2,140 kg·m⁻³, as used by Sjaardema and Krieg [1987] and Butcher et al. [1991].

The bentonite used in the samples was a granular MX-80 Volclay bentonite commercially available from the American Colloid Company of Belle Fourche, South Dakota, and is described in greater detail elsewhere [Pfeifle, 1987]. This product is identical to the material used in backfill studies at the WIPP. The as-received water content of the bentonite was 6.97 percent by dry weight as determined from the drying method described above. The assumed solid density of the bentonite was 2,700 kg·m⁻³ [Butcher et al., 1991].

The brine used in this study was a synthetic brine prepared by Twin Cities Testing, Rapid City, South Dakota. The brine had a final composition that simulated Brine A, a naturally occurring WIPP brine that is high in magnesium. Small amounts of finely crushed WIPP salt were added to this brine to ensure that the solution was fully saturated. The brine was 67.89 percent by weight water and 32.11 percent by weight dissolved solids.

2.2 PREPARATION

2.2.1 Sample

Four separate sample batches of crushed salt, bentonite, and brine were prepared for use in fabricating the four test specimens used in this study. Shortly before each specimen was to be fabricated, a sample batch was prepared by first mixing the proper predetermined masses of “as-received” crushed salt and bentonite in a large flat container and then adding the correct mass of brine to the mixture to yield the nominal water content for the test. The description “as-received” denotes materials that contain both solids and some initial amount of water as described previously in Section 2.1. The mass of brine added to the mixture was adjusted to compensate for both the initial water content of the “as-received” materials and the water-to-dissolved solids ratio of the brine. This method produced sample batches of 70 percent by dry weight of crushed salt and 30 percent by dry weight of bentonite and yielded a dry mass of 3,000 g for each of the four sample batches. The theoretical solid density of the batches was $2,282 \text{ kg}\cdot\text{m}^{-3}$.

The total or wet masses (including solids and water) among the sample batches varied depending on the nominal water content and, in all cases, exceeded the dry batch mass of 3,000 g. Although the wet mass of the sample batches exceeded 3,000 g, only approximately 2,500 g (wet) were required to fabricate each specimen. The larger sample batch provided sufficient material to determine the actual water content of each batch. Three water content determinations were made for each batch after the materials had been mixed thoroughly and before the specimens were fabricated. These determinations were made using the drying procedure described in Section 2.1 and were averaged to provide the water content values shown in Table 1-1. The remainder of each sample batch was weighed and then temporarily stored in a sealed container to prevent moisture loss before the test specimens were fabricated. All mass determinations were made using a Sartorius balance having a resolution of 0.01 g.

2.2.2 Specimen

Specimens that were 101.6 mm in diameter and 203 mm in length were constructed as shown in Figure 2-1. A 1.6-mm-thick lead inner jacket protected the outer Viton jacket that was used to seal against the confining pressure oil. Scotchbrite was placed between each platen and the specimen to provide a high-permeability interface between the platen with its central pore-fluid vent and the test specimen. Scotchbrite is a tradename for 3M’s nylon-web pad impregnated with aluminum oxide and is used in industry as a cleaning and deburring pad for metals and ceramics. The cylindrical volume created by the jackets and platens was filled with the proper batch sample using five equal layers each tamped lightly with a 3-mm-diameter rod to remove any trapped air voids. When the space was filled,

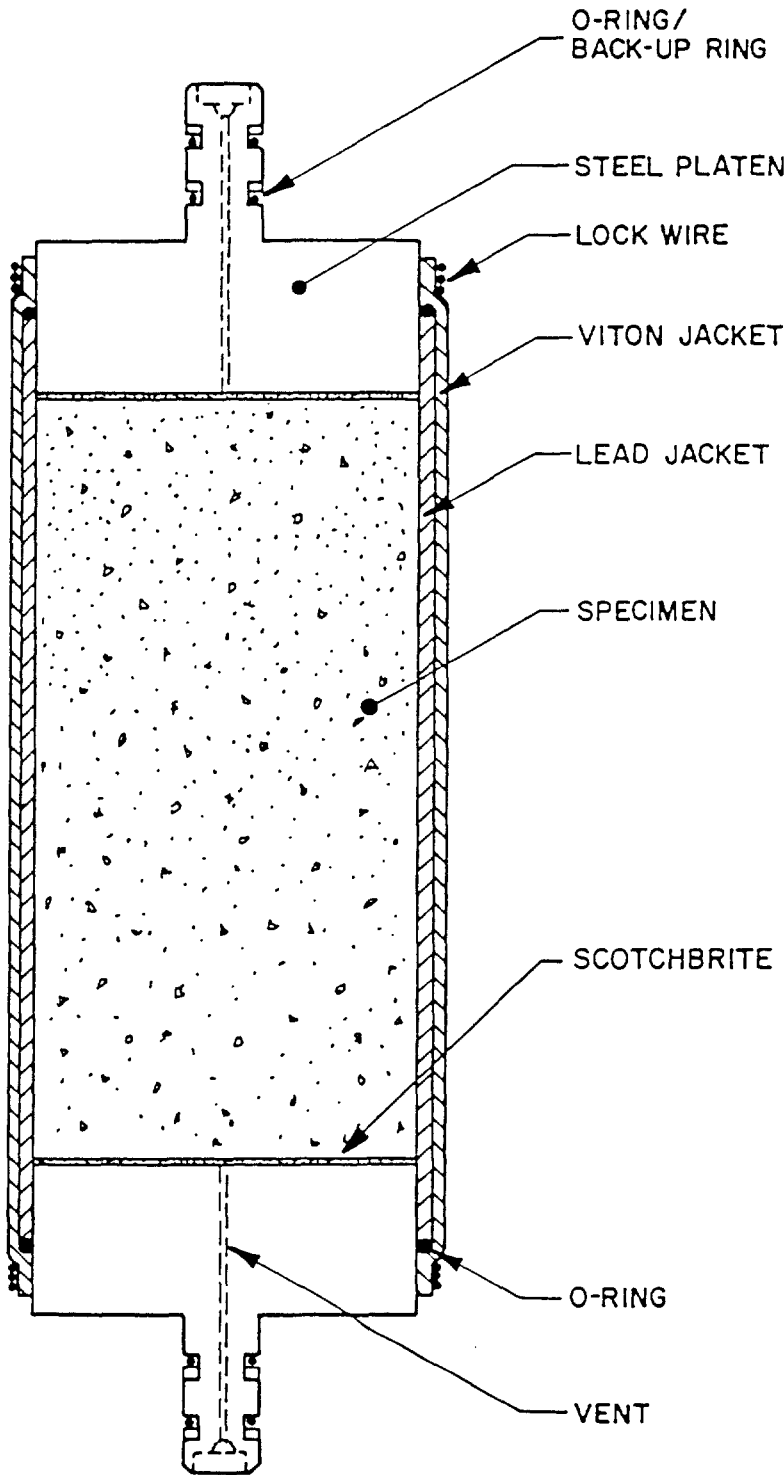
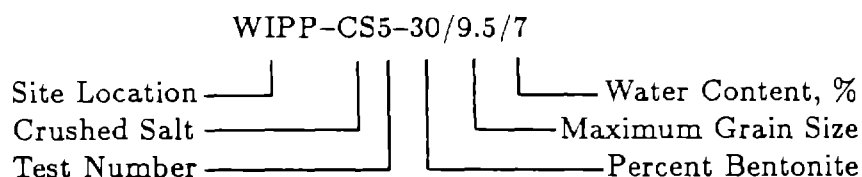


Figure 2-1. Specimen assembly.

the wet mass of the specimen was determined indirectly by weighing the amount of the batch sample remaining in the original sample container using the Sartorius balance. This procedure allowed accurate determination of the starting mass and thus the density of the specimen.

Each specimen was assigned an identification number and logged into the RE/SPEC sample inventory. A typical identification number is as follows:



Abbreviated specimen numbers are used throughout the remainder of the report. Table 2-1 gives the correlation between complete and abbreviated identification numbers and the water contents for each specimen.

Table 2-1. Specimen Identification Numbers

Complete	Abbreviated	Nominal Water Content	
		Dry Wt. (%) ^(a)	Total Wt. (%) ^(a)
WIPP-CS5-30/9.5/7	CS5	7.47 ± 0.21	6.95±0.20
WIPP-CS6-30/9.5/10	CS6	10.85 ± 0.65	9.79±0.59
WIPP-CS7-30/9.5/3.5	CS7	3.38 ± 0.28	3.27±0.27
WIPP-CS8-30/9.5/7	CS8	7.46 ± 0.21	6.94±0.20

(a) Standard deviation based on scatter of three values about the mean.

2.3 POST-TEST DISPOSITION

As the tests were completed, specimens were sealed in plastic bags and returned to the RE/SPEC core storage facilities. The specimen from Test CS5 was sectioned immediately after the unconfined compressive strength test was performed to obtain eight samples for final water content determinations. Each section was broken into smaller aggregations before being placed into the drying ovens used for the water content determinations. Therefore, this specimen in storage contains eight smaller aggregations of dried particles. The remaining specimens were stored intact in air-tight bags.

3.0 TEST APPARATUS

3.1 CONSOLIDATION

3.1.1 Load Frame

Figure 3-1 presents a cross section of a typical creep testing load frame with prominent components labeled for reference. They are nearly identical to those used by Holcomb and Hannum [1982] at Sandia National Laboratories. The machines use a single-ended, triaxial pressure vessel that accommodates a 108-mm-diameter cylindrical specimen having a length-to-diameter ratio of $L:D = 2$ to 2.5. A linear actuator (hydraulic cylinder) bolted to the base of the load frame drives the loading piston, which applies axial compressive force to the specimen. Confining pressure is applied to the jacketed specimen by pressurizing the sealed vessel chamber with silicone oil. A dilatometer system maintains constant confining pressure and provides the volumetric measurement.

The testing machines can apply compressive axial loads up to 1.5 MN and confining pressures up to 70 MPa. The heating system, including seals on the pressure vessel, can maintain specimen temperatures up to 200°C.

A control panel houses the accumulators, hydraulic pumps, pressure intensifiers, transducer signal conditioners, temperature controllers, and confining pressure controllers for two adjacent test frames. The panels contain digital meters that display the output of the transducers. The temperature controller gives a digital output of the temperature. Mechanical pressure gauges mounted in the panel give readings of the oil pressure in the hydraulic cylinder.

3.1.2 Instrumentation

Axial force is measured by a load cell in the load train outside the pressure vessel, while confining pressure is measured by a pressure transducer in the line between the intensifier and the pressure vessel. Temperature is measured by a thermocouple in the wall of the pressure vessel. The relationship between specimen temperature and that recorded by this thermocouple has been determined by calibration runs at several temperatures spanning the operating range. Two Linear Variable Differential Transformers (LVDTs) mounted outside the pressure vessel monitor displacement of the loading piston relative to the bottom of the pressure vessel. Volumetric deformation is measured using a dilatometer. With this technique, volumetric deformation is determined at fixed pressure by first measuring the volume of oil that the intensifier supplies to the pressure vessel and then compensating for the volume of oil displaced by the axial piston as measured by the LVDTs. A rotary potentiometer or stroke transducer is mounted on the intensifier

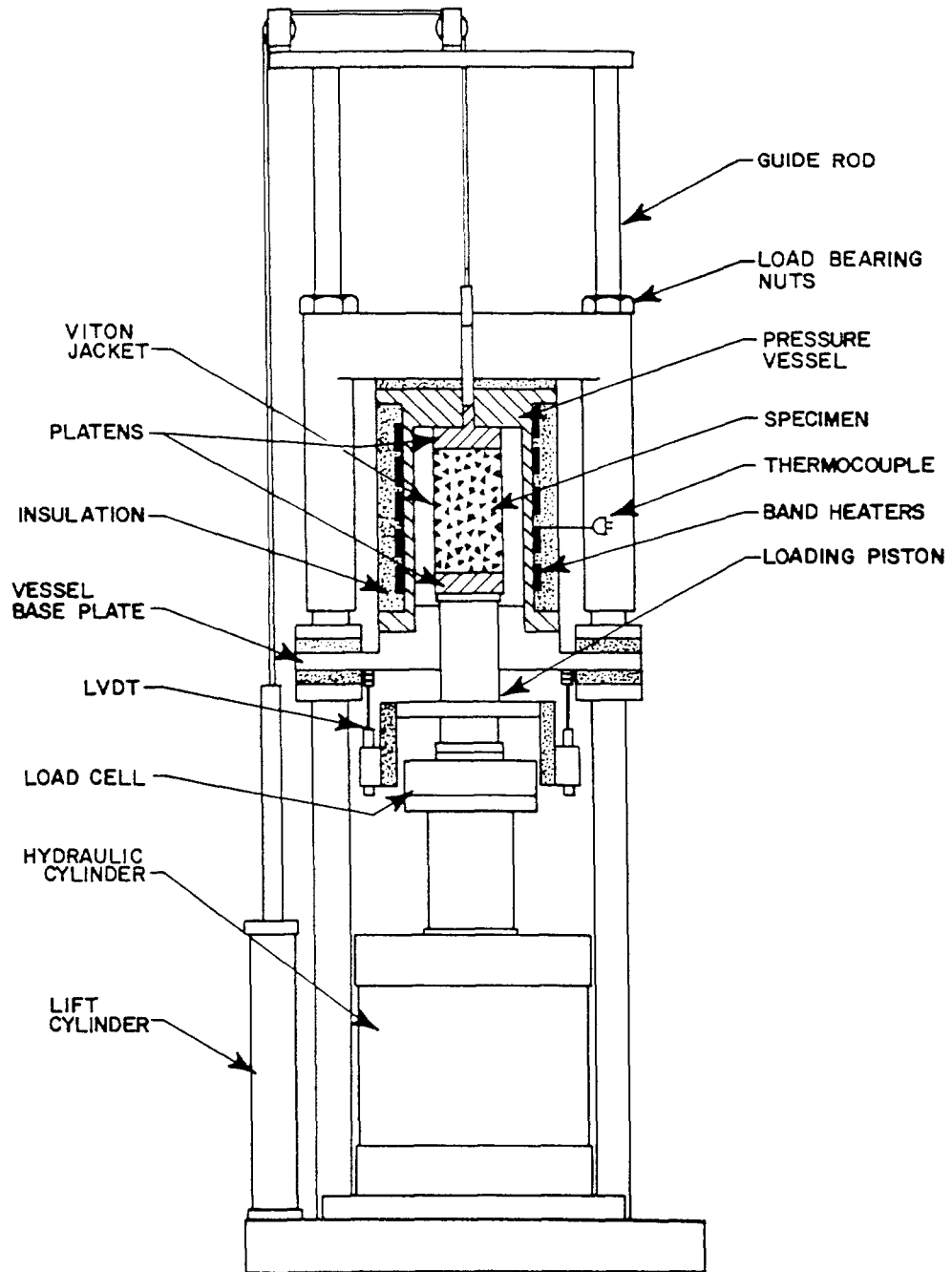


Figure 3-1. Testing frame for consolidation tests.

shaft to provide a signal proportional to the volume of oil supplied to the pressure vessel.

3.1.3 Control

Temperature is maintained with a manual set point controller that regulates power to the band heaters on the vessel. The thermocouple in the pressure vessel wall supplies the feedback signal. The specimen temperature is maintained constant within 0.2°C. Confining pressure is controlled by inputting the pressure transducer signal to a unit that contains two manual set points. These set points are adjusted to maintain the confining pressure constant within 20 kPa. The controller signals the intensifier to advance or retreat depending upon whether the lower or upper set point has been reached. A standby diesel generator provides electrical power to the test system during periods of commercial electrical power outages.

3.2 PERMEABILITY

Figure 3-2 shows a schematic of the apparatus used for the brine permeability measurements. In this apparatus, an accumulator is connected hydraulically to the specimen via stainless-steel tubing and the vent in the lower end platen. The accumulator is filled with brine and charged with nitrogen using a standard nitrogen bottle. The charge pressure (and therefore the pressure drop across the specimen) is regulated manually with a valve located on the nitrogen bottle and is measured using a diaphragm-type pressure transducer in the line between the nitrogen bottle and the accumulator. Brine flow through the specimen is captured and measured by a buret attached to the upper end platen of the specimen. Evaporation of water is controlled by placing a thin film of mineral oil on top of the brine column in the buret.

3.3 STRENGTH

3.3.1 Load Frame

Figure 3-3 shows a schematic of the two-column load frame used to perform the unconfined compressive strength test. A pressure vessel is shown in the figure; however, confining fluid was not used for this test. The frame and load actuator located in the base of the machine can apply 500 kN of force to a specimen. The movable crosshead allows for a wide range of specimen lengths and a variety of tests.

A control console houses all signal conditioning for the transducers, as well as feedback and valve driver modules for the hydraulics. This console interfaces with

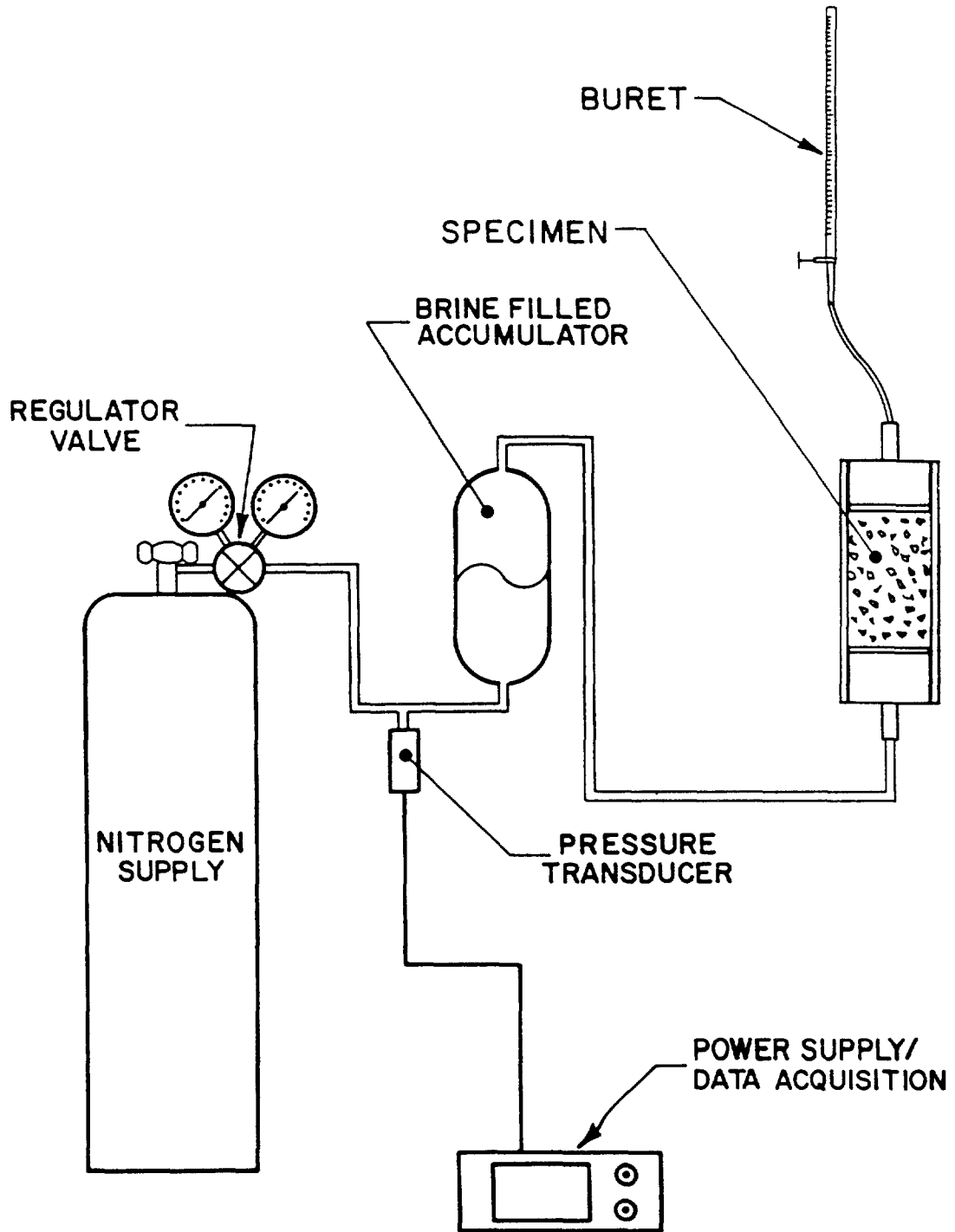
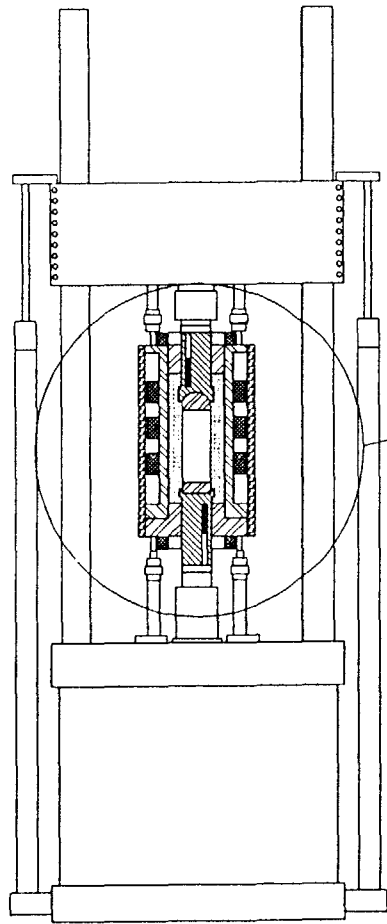
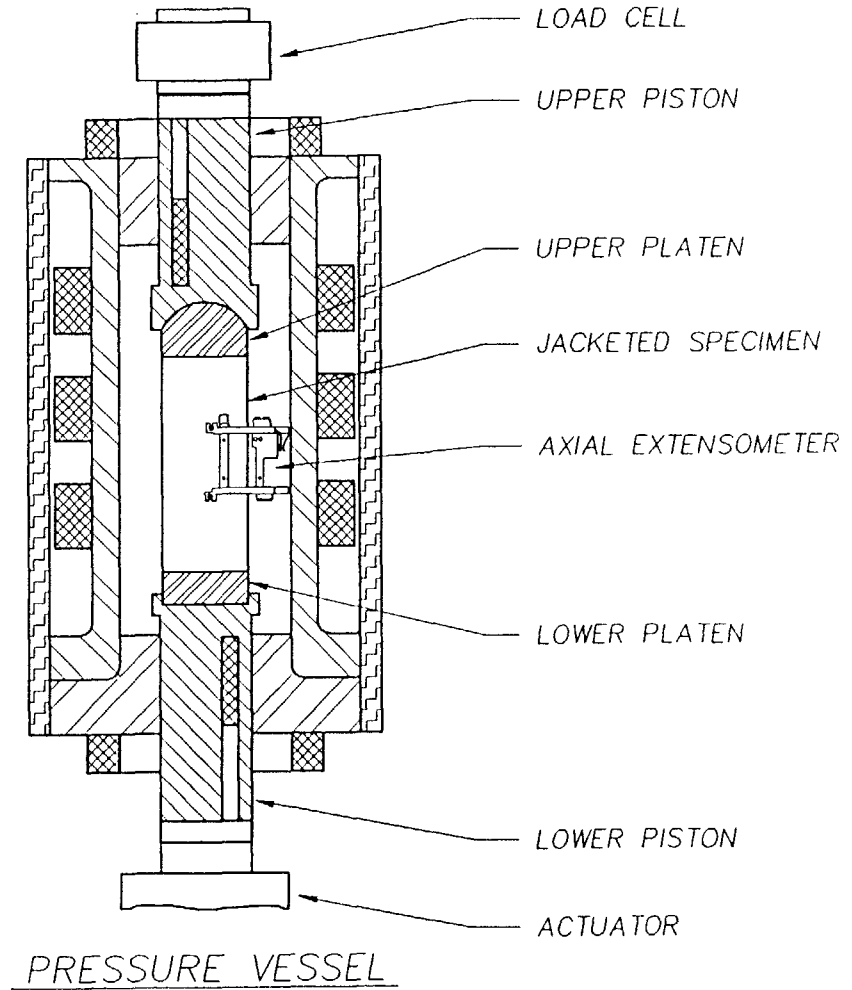


Figure 3-2. Schematic of brine permeability test system.



LOAD FRAME



RSI-183-91-01

Figure 3-3. Test frame for constant strain-rate tests.

a DEC LSI-11/73 microprocessor to provide data acquisition and programmable control.

3.3.2 Instrumentation and Control

Two types of transducers were required for this test: a load cell and a direct contact axial extensometer. The load cell is mounted on the movable crosshead and provides force measurements. The extensometer, an MTS 632.90C-04 strain-gauge-type consists of two sensing arms each 100 mm long and mounted 180 degrees apart, provides a measurement of average strain. This gauge was centered with respect to the specimen midheight. The ambient laboratory temperature during the tests was $20^{\circ} \pm 1^{\circ}\text{C}$.

3.4 CALIBRATION

All transducers were calibrated in their normal operating positions on the test system, and outputs were observed at normal data collection points. By using this approach, the signal conditioners, filters, and analog-to-digital converters were all included within the "end-to-end" calibration. Known input levels to the calibration system were provided by NIST (National Institute of Standards and Technology) traceable standards maintained in the RE/SPEC Inc. metrology laboratory. Calibrations for pressure and displacement were performed by determining the best straight-line fits to indicated readings versus standard input after applying the standard input in 20 equal steps. The calibration constants were then verified by applying the standard input in 10 equal steps over the calibrated range. The transducer response at each step was predicted using the calibration constants. The process of calibration/verification was repeated until the predicted values fell within acceptable levels of error: 1.0 percent of reading for force, pressure and volume calibrations, and 2.0 percent of reading for displacement calibrations. Table 3-1 gives the range and resolution for all transducers. The burets used were Class A and have an accuracy of better than 0.1 ml.

Table 3-1. Transducer Ranges and Resolutions

Measurement	Range	Resolution
CONSOLIDATION		
Axial Deformation (mm)	0 to 25.4	0.0016 ^(a)
Lateral Strain (%)	0 to 8	0.002 ^(a)
Axial Load (kN)	0 to 250	0.03 ^(a)
Confining Pressure (MPa)	0 to 34.5	0.004 ^(a)
Temperature (°C)	0 to 250	0.03 ^(a)
PERMEABILITY		
Pressure (kPa)	0 to 345	0.69 ^(b)
STRENGTH		
Axial Deformation (mm)	0 to 7.5	0.00092 ^(a)
Force (kN)	0 to 50	0.006 ^(a)

(a) 14-bit analog-to-digital converter with one bit for sign.

(b) 4-1/2-digit panel meter.

4.0 TEST PROCEDURES

4.1 DENSITY

A determination of specimen density was required before and after each stage of each test. Density requires measurements of both mass and volume. Mass was measured using a Sartorius balance. Volume was determined using two techniques: (1) fluid (water) displacement and (2) indirect dimensional measurement. Volumetric measurements in both techniques were performed while the specimen was subjected to a vacuum of approximately 630 mm of mercury. The vacuum was used to remove air trapped between the jacketing materials and the specimen and at other component interfaces. The temperature during the measurements was $20^{\circ} \pm 1^{\circ}\text{C}$.

In the fluid displacement technique, the volume of the jacketed specimen was determined by measuring the weight of water displaced when the specimen was submerged in a container equipped with an overflow spout and converting the weight to volume using the specific gravity of the fluid. The volume of the specimen was then determined by subtracting the volumes of the nonspecimen components from this displaced volume. The volumes of the platens, jackets, O-rings, and lock-wire were determined from their masses and specific gravities. The volume of the Scotchbrite depends on the applied vacuum, and was therefore determined by using an aluminum cylinder of known dimensions in place of the specimen, then evacuating the specimen assembly and measuring its volume.

In the indirect measurement technique, specimen volume was determined from the length and diameter of the specimen assuming a right-circular, solid cylinder configuration. The diameter of the specimen was determined by first measuring the diameter of the jacketed specimen at six locations using a micrometer and then reducing the measurements by twice the lead and Viton jacket thicknesses. Similarly, the length of the specimen was determined by measuring the height of the jacketed specimen using a gauge head and transfer standard and then subtracting the lengths of the end platens and the thickness of the Scotchbrite from this measured height. Again, the thickness of the Scotchbrite was measured using an aluminum specimen under vacuum. This technique yielded volumes within 3 percent of those determined using the fluid displacement technique, even though the highly deformed specimens caused the jacketing to deform unevenly and produce large wrinkles.

4.2 CONDITIONING

Because of the rapid consolidation expected during hydrostatic loading of the specimens and the inability of the test system to measure volumetric displacements under nonconstant pressure, all specimens were conditioned before beginning the first two stages of each test. The conditioning provided a measurement of the change in density during loading, before the start of time-dependent consolidation.

Conditioning was not required before the third stage of each test because it was conducted at a lower pressure than the previous stage, and no further consolidation was expected during hydrostatic compression. The conditioning consisted of placing the specimen in the load frame, loading the specimen to the desired conditioning pressure, and then unloading the specimen immediately. The conditioning pressure was the prescribed pressure of the following consolidation stage as given in Table 1-1. The specimen was removed from the load frame following each conditioning and its volume was measured using both measurement techniques described previously.

The effect of conditioning on specimen density is shown in Table 4-1. In general, the conditioning procedure increased the density of the specimens at each stage; however, in one instance (CS6, Stage 2), the density decreased by a very small amount. This decrease is thought to have resulted from specimen swelling and probably only occurred because of a delay between removing the specimen from the pressure vessel after conditioning and making the volume measurement. The change in density during conditioning can vary considerably as seen in Table 4-1 and shown by comparing Tests CS5 and CS8. These tests had the same moisture contents but compacted by 5.9 and 14.6 percent, respectively, during the conditioning for Stage 1. Test CS8 had the lowest initial density and so a high degree of compaction was expected for this stage; however, it compacted to a higher density than any of the other tests. While there is no reason to disregard the conditioning data from Test CS8, the change in density associated with Stage 1 conditioning is an outlier, and if that test is omitted, then the remaining tests show a correlation between density change during the Stage 1 conditioning and moisture content.

4.3 CONSOLIDATION

The four consolidation tests were performed in stages. Before each stage was initiated, the specimen was conditioned as described above. After the density of the conditioned specimen was determined, it was returned to the load frame, the pressure vessel was lowered, and the loading piston was advanced far enough to engage the top platen pressure seal, but not so far that the platen contacted the top of the pressure vessel. This positioning ensured that the specimen was not subjected to an axial stress difference imposed by the piston during consolidation. The supply line to the hydraulic cylinder was then closed so that the piston position was maintained. The pressure vessel was filled with silicone oil and heated to 25°C. After temperature stabilization (~24 hours), the desired consolidation pressure for the stage was applied in approximately 30 seconds by pressurizing the oil with an air-driven pump. Data acquisition began when the prescribed pressure was reached and control of the pressure was given to the automatic controller.

The lower platen vent was plugged during consolidation; however, the upper vent was equipped with a flexible tube containing a brine trap. The trap allowed air to escape but prevented evaporation from the specimen during consolidation.

Table 4-1. Densities Before and After Conditioning

Test I.D.	Moisture Content (Dry Wt. %)	Dry Density (kg·m ⁻³)		$\Delta\rho^{(a)}$ (%)
		Initial	Conditioned	
CS5 Stage 1	7.47	1,384	1,466	+5.9
Stage 2		1,669	1,696	+1.6
CS6 Stage 1	10.85	1,381	1,485	+7.5
Stage 2		1,803	1,794	-0.4
CS7 Stage 1	3.38	1,424	1,493	+4.8
Stage 2		1,578	1,620	+2.7
CS8 Stage 1	7.46	1,349	1,547	+14.7
Stage 2		1,704	1,730	+1.5

(a) Change in dry density.

Depending on the amount of specimen consolidation, the piston could be advanced during the test to maintain the platen-vessel seal at the top of the vessel. The volumetric data collected by the potentiometer or stroke transducer were corrected to account for piston motion into or out of the pressure vessel since piston position is recorded using the LVDTs.

The data acquisition computer was programmed to scan the data channels at 15-second intervals. Data were logged by the computer for each 0.02 mm of axial deformation or every hour if the axial deformation was less than 0.02 mm in a 1-hour interval. Recorded data were written to disk by the data acquisition computer and transmitted to a larger computer for analysis.

4.4 PERMEABILITY

A permeability test was performed once the specimen had consolidated so that it was fully saturated at the prescribed water content. The theoretical saturated wet density of the specimen was calculated from simple volume-density relationships assuming complete interconnectivity of voids using

$$\rho_{sat}^w = \frac{G\rho_w(1+w)}{1+wG} \quad (4-1)$$

where

- ρ_{sat}^w = Saturated wet density (having units ML^{-3})
- G = Specific gravity¹ of solids (unitless)
- ρ_w = Density of water (having units ML^{-3})
- w = Water content expressed as a fraction of dry weight (unitless)

When the density of the specimen reached this theoretical density, the test stage was stopped, the pressure dropped, and the specimen removed to determine its density. The specimen was then returned to the same testing machine and a partially filled buret was connected to the outlet of the specimen using a flexible hose. The prescribed confining pressure of 0.5 MPa was then applied to the specimen.

Permeability was determined by measuring the steady flow rate of brine through the specimen and the pressure drop across the specimen under hydrostatic conditions. The pressure drop was maintained at 345 kPa during the test. The flow rate was determined by monitoring the level of brine in the buret with time.

4.5 STRENGTH

After the permeability stage had been completed for Test CS5, an unconfined compressive strength test was performed. Before the test was performed, the specimen was removed from the creep testing load frame, its density determined, and its Viton and lead jackets removed. The consolidation pressures were sufficient to deform the lead jacket into the surface voids of the specimens. When the jacket was removed, some salt grains remained embedded in the lead jacket. Although some grains were removed from the surfaces of the specimens and the specimen deformation was not entirely uniform over the length of the specimen, measurements of the average diameter and length of the specimens were made using a micrometer and gauge head and transfer standard, respectively.

The specimen was fitted with a loosely fitting plastic sleeve to prevent moisture loss and mounted in the two-column load frame. A direct contact axial deformation extensometer was attached to the specimen. During the test a small axial preload was applied manually to the test specimen and then a uniaxial constant axial strain-rate test was performed at ambient temperature ($20^\circ \pm 1^\circ\text{C}$). The axial extensometer was also used as the feedback signal for control. The test proceeded at a nominal rate of $10^{-5} \cdot \text{s}^{-1}$ until peak load was achieved, at which time the specimen was unloaded. Force and strain data were recorded during loading. Peak load and the average initial specimen diameter were used to calculate the unconfined compressive strength.

¹Specific gravity, defined as the ratio of the mass of a unit volume of a material to the mass of the same volume of water at a given temperature, was calculated using the theoretical densities of salt and bentonite and assuming a density of water of $1,000 \text{ kg m}^{-3}$. The specific gravity of the solids of a 70/30 crushed salt/bentonite mixture is 2.282.

4.6 WATER DISTRIBUTION

The water distribution parallel to the specimen axis was determined for Test Specimen CS5 after the strength test was performed. Eight samples were obtained by sectioning the specimen with a hacksaw. Cuts were made perpendicular to the specimen axis and were spaced so as to yield samples of approximately the same mass. The samples were then broken up into smaller aggregations and dried in an oven at 110°C for 6 days according to the drying procedure given in Section 2.1.

5.0 TEST RESULTS

5.1 CONSOLIDATION

During each test, the change in specimen volume was continuously measured using a dilatometer. From this data and the specimen mass and volume determined as described in Section 4.1, volumetric strain, density, and fractional density were determined. Elastic strains resulting from pressure changes were assumed to be small compared to the inelastic strains and were ignored in all analyses.

5.1.1 Volumetric Strain

The engineering strain definition was used to calculate volumetric strain, ϵ_v , as

$$\epsilon_v = \frac{\Delta V}{V_o} \quad (5-1)$$

where ΔV was the change in specimen volume and V_o was the original specimen volume. Figures 5-1 to 5-4 give the total volumetric strains for Tests CS5, CS6, CS7, and CS8, respectively, and include both the conditioning and the consolidation strains. The durations of the tests (including permeability) ranged from 65 to 118 days. Test CS5 was terminated just after the initiation of the permeability stage because a channel formed in the lead jacket that surrounded the specimen, invalidating permeability measurements. The specimen was used later for strength and moisture content measurements. Test CS7 was terminated after Stage 2 because at this low moisture content, the consolidation rate was too slow to attain the saturated density and allow completion of the test.

During the second stage of a test, the pressure was increased to acquire volumetric strain-time data at a higher pressure and also to reduce the time required to reach saturation. The apparent drop in volumetric strain at the start of Stage 2 of CS6 (Figure 5-2) is caused by the method used to calculate volumetric strain. Volumetric strain during Stage 1 was calculated from the specimen volume at the beginning of the stage and the dilatometer data. At the end of the stage, volumetric strain was remeasured using the fluid displacement technique. Since this technique provides a more accurate measurement of volume than the dilatometer method, the volumetric strain was adjusted to the new value. In the case of Test CS6, the new value was lower than the previous value. Density measurements performed at the end of each creep stage were within 3 percent of those determined from the pre-creep density measurements and the volumetric strain data recorded by the dilatometer. The only exception to this was Stage 2 of Test CS7 (Figure 5-3), which had a discontinuity in strain measurements at approximately 48 days caused by a drop in confining pressure. The pressure returned to its nominal value after one day. The

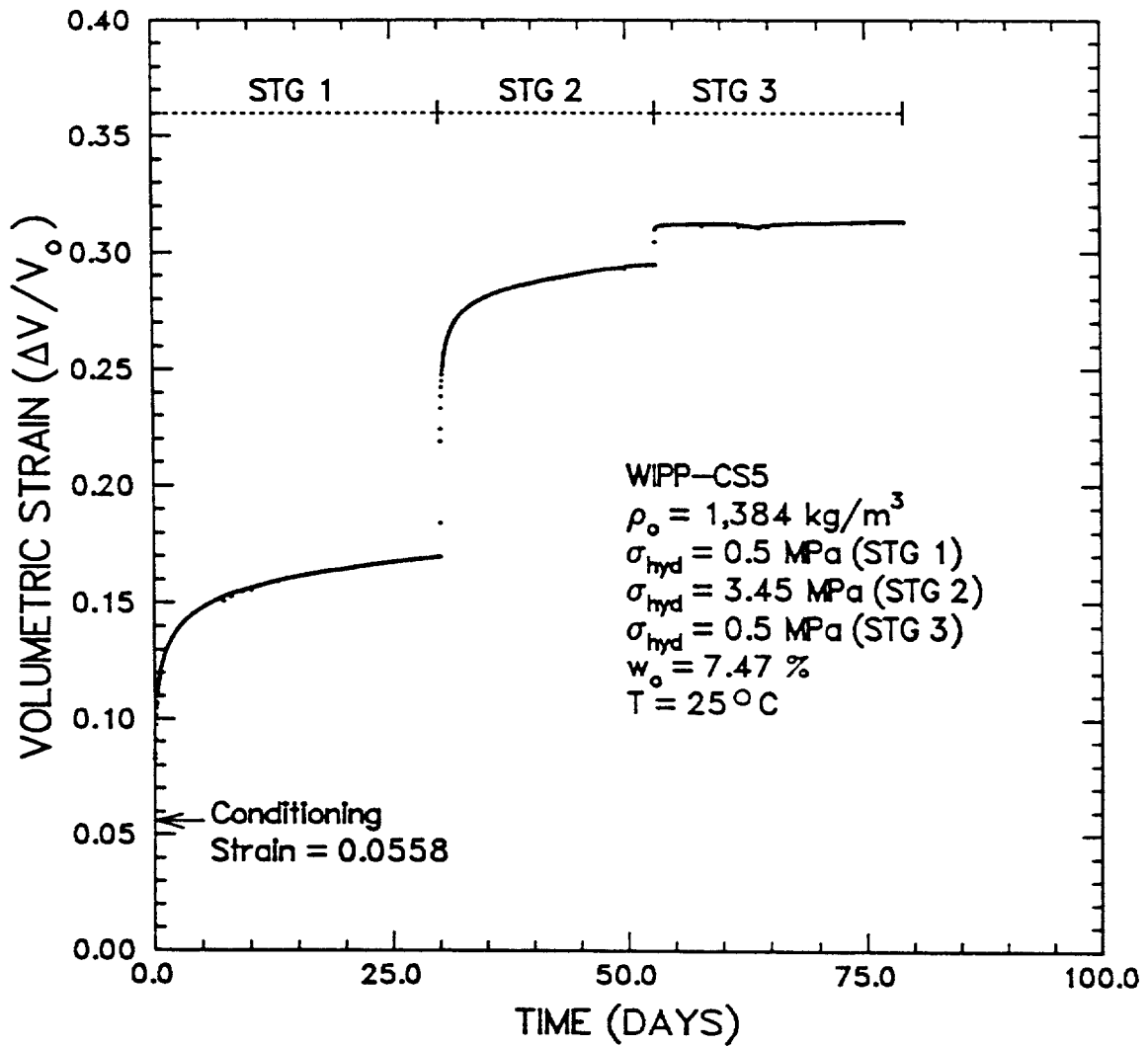


Figure 5-1. Volumetric strain-versus-time for WIPP-CS5, 70/30 crushed salt/bentonite.

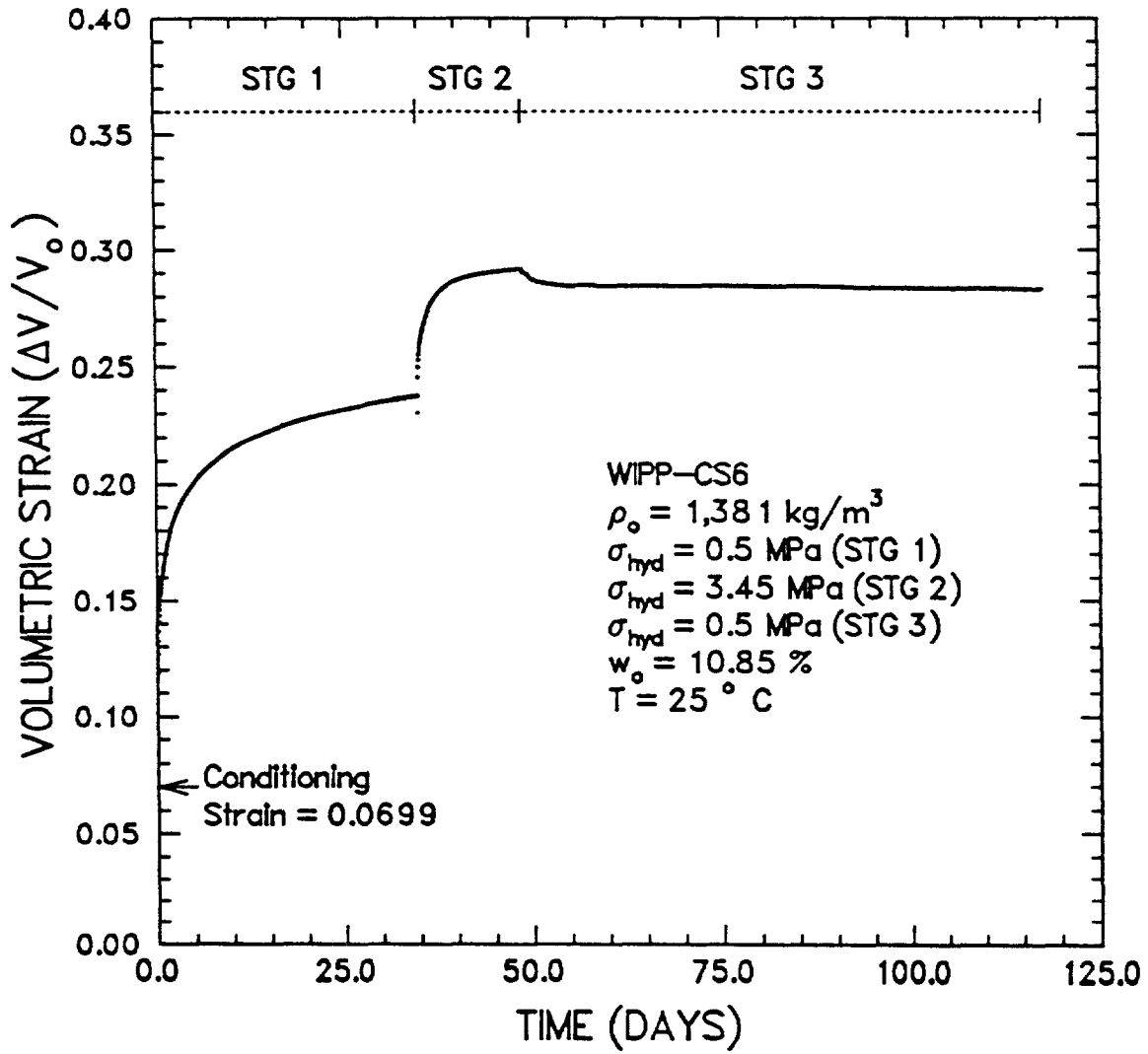


Figure 5-2. Volumetric strain-versus-time for WIPP-CS6, 70/30 crushed salt/bentonite.

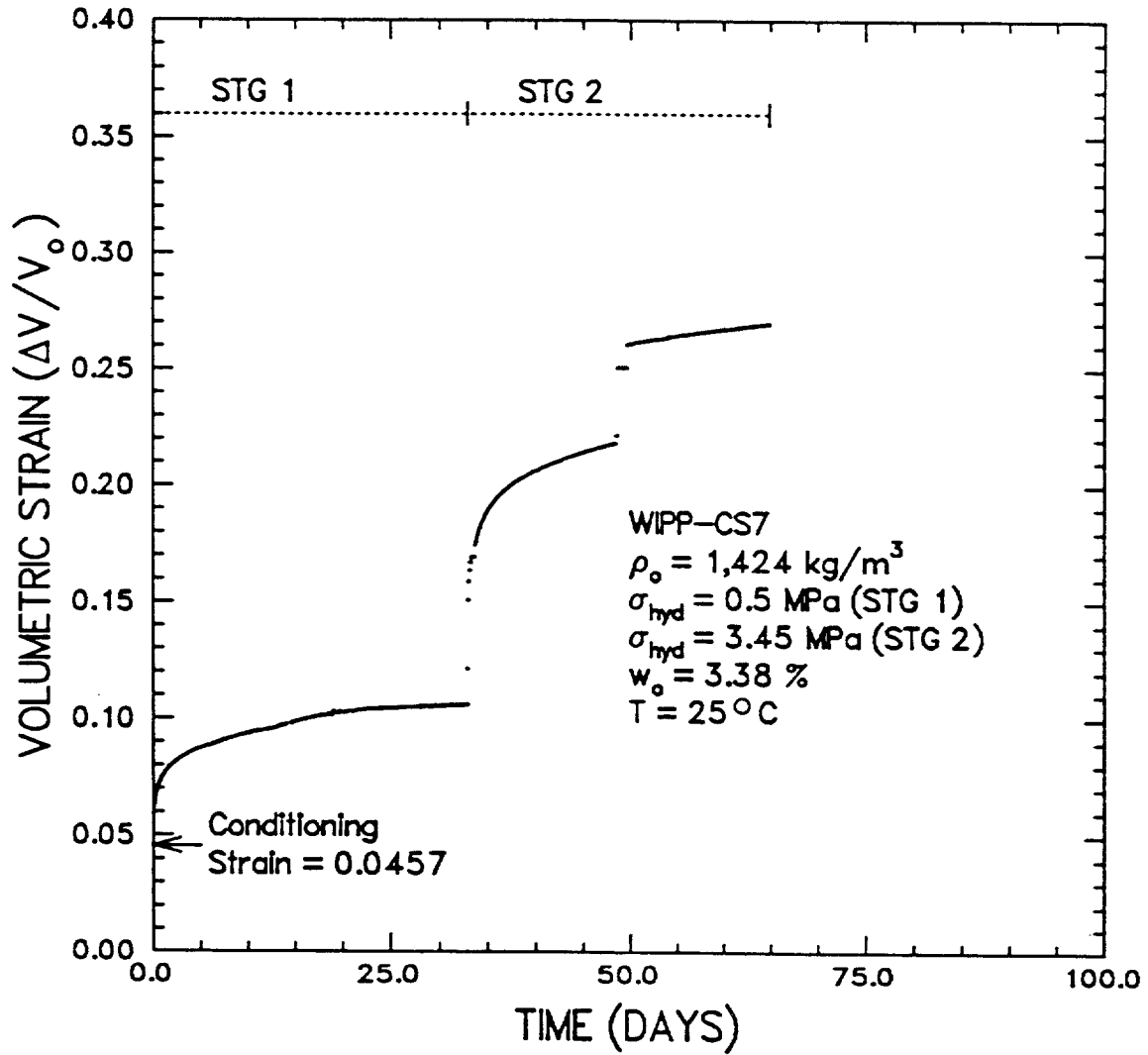


Figure 5-3. Volumetric strain-versus-time for WIPP-CS7, 70/30 crushed salt/bentonite.

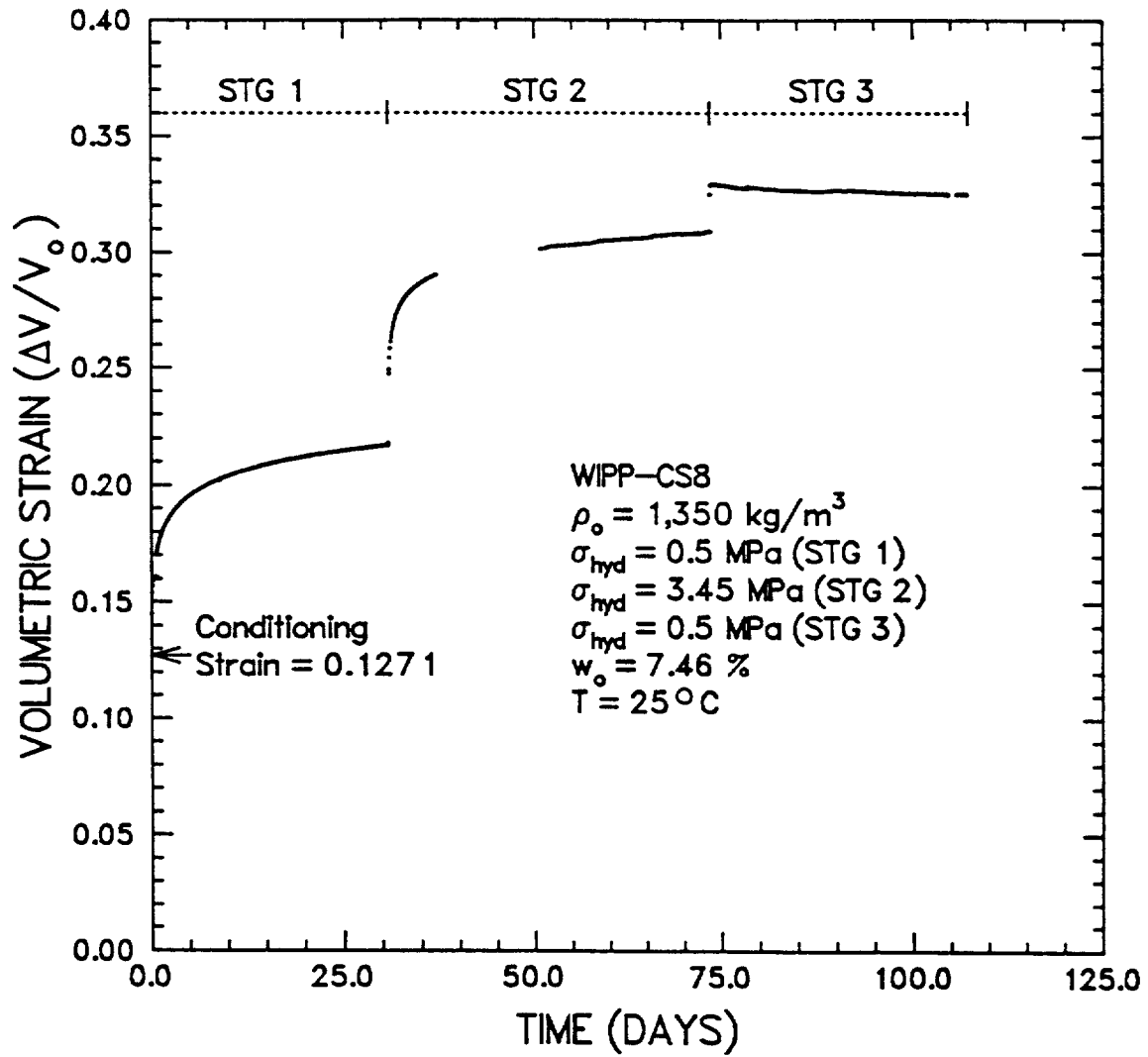


Figure 5-4. Volumetric strain-versus-time for WIPP-CS8, 70/30 crushed salt/bentonite.

gap in the data during Stage 2 of CS8 (Figure 5-4) was due to disk failure in the computer controlling the test. In all tests, the pressure during the third stage of the test (permeability) was 0.5 MPa, which is lower than the previous stage. As seen in Figures 5-1 through 5-4, little additional volumetric strain was measured during the final stage at the reduced pressures. In fact, the total volumetric strain decreased in Tests CS6 and CS8 indicating that some swelling occurred immediately after the pressure was reduced.

5.1.2 Density

Density was determined as a function of time to monitor the saturation level during the test and to provide data for model fitting and fractional density determinations. The wet density, ρ^w , was calculated from the wet mass, M^w , and the current volume as

$$\rho^w = \frac{M^w}{V} \quad (5-2)$$

This density was compared to the theoretical saturated density (Equation 4-1) to determine when the specimen reached full saturation. The dry density, ρ^d , was calculated as

$$\rho^d = \frac{\rho^w}{1 + w} \quad (5-3)$$

where w is the water content expressed as a fraction.

Fractional density was calculated from the dry density using

$$D = \frac{\rho^d}{\rho^{th}} \quad (5-4)$$

where ρ^{th} is the theoretical solid density of the mixture equal to 2,282 kg·m⁻³. A summary of density information is provided in Table 5-1.

For tests in which water was expelled from the specimen during Stages 2 and 3, the dry density was calculated from Equation 5-3 using a corrected water content. This corrected water content was calculated assuming that after saturation was reached, all volume changes resulted in the expulsion of an identical volume of brine. Dry and wet density-time curves for all stages of each test are given in Figures 5-5 through 5-8.

Table 5-1. Summary of Density Data for Creep Consolidation Tests^(a)

Test ID	Water Content ^(b) (Dry Wt %)	Hydrostatic Stress ^(c) (MPa)	Dry Density (kg · m ⁻³)			Fractional Dry Density ^(d)		
			ρ_{initial}	$\rho_{\text{conditioned}}$	$\rho_{\text{post-creep}}$	D_{initial}	$D_{\text{conditioned}}$	$D_{\text{post-creep}}$
CS 5								
Stage 1	7.47	0.5	1,384	1,466	1,669	0.606	0.642	0.731
Stage 2	7.47	3.45	1,669	1,696	1,983	0.731	0.743	0.869
Stage 3 ^(e)	6.63 ^(f)	0.5	1,983	(g)	1,963	0.869	(g)	0.860
CS 6								
Stage 1	10.85	0.5	1,381	1,485	1,803	0.605	0.651	0.790
Stage 2	10.85	3.45	1,803	1,794	1,926	0.790	0.786	0.844
Stage 3 ^(e)	8.14 ^(f)	0.5	1,926	(g)	1,956	0.844	(g)	0.857
CS 7								
Stage 1	3.38	0.5	1,424	1,493	1,577	0.624	0.654	0.691
Stage 2	3.38	3.45	1,577	1,620	1,858	0.691	0.710	0.814
CS 8								
Stage 1	7.46	0.5	1,350	1,547	1,704	0.592	0.678	0.747
Stage 2	7.46	3.45	1,704	1,726	1,989	0.745	0.756	0.872
Stage 3 ^(e)	6.32 ^(f)	0.5	1,989	(g)	1,927	0.872	(g)	0.845

(a) All data were calculated based on direct measurements of volume made using the fluid displacement technique.

(b) Water content at start of stage.

(c) Hydrostatic stress and conditioning pressure are identical.

(d) Based on theoretical intact density of 2,282 kg · m⁻³.

(e) Permeability stage.

(f) Water content is corrected for volume of brine that was squeezed out of specimen after saturation.

(g) No conditioning was required.

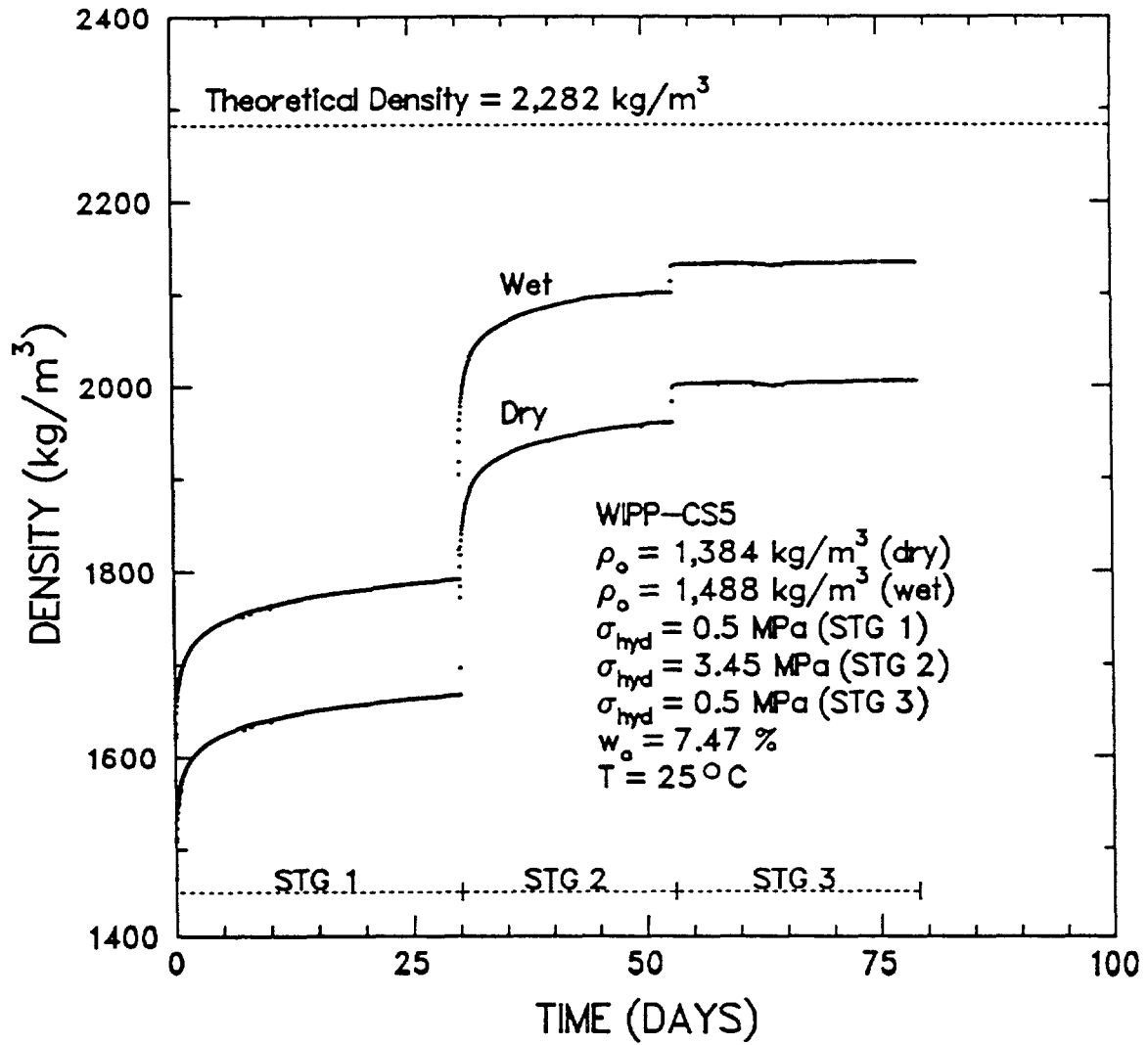


Figure 5-5. Wet and dry density as a function of time for WIPP-CS5, 70/30 crushed salt/bentonite.

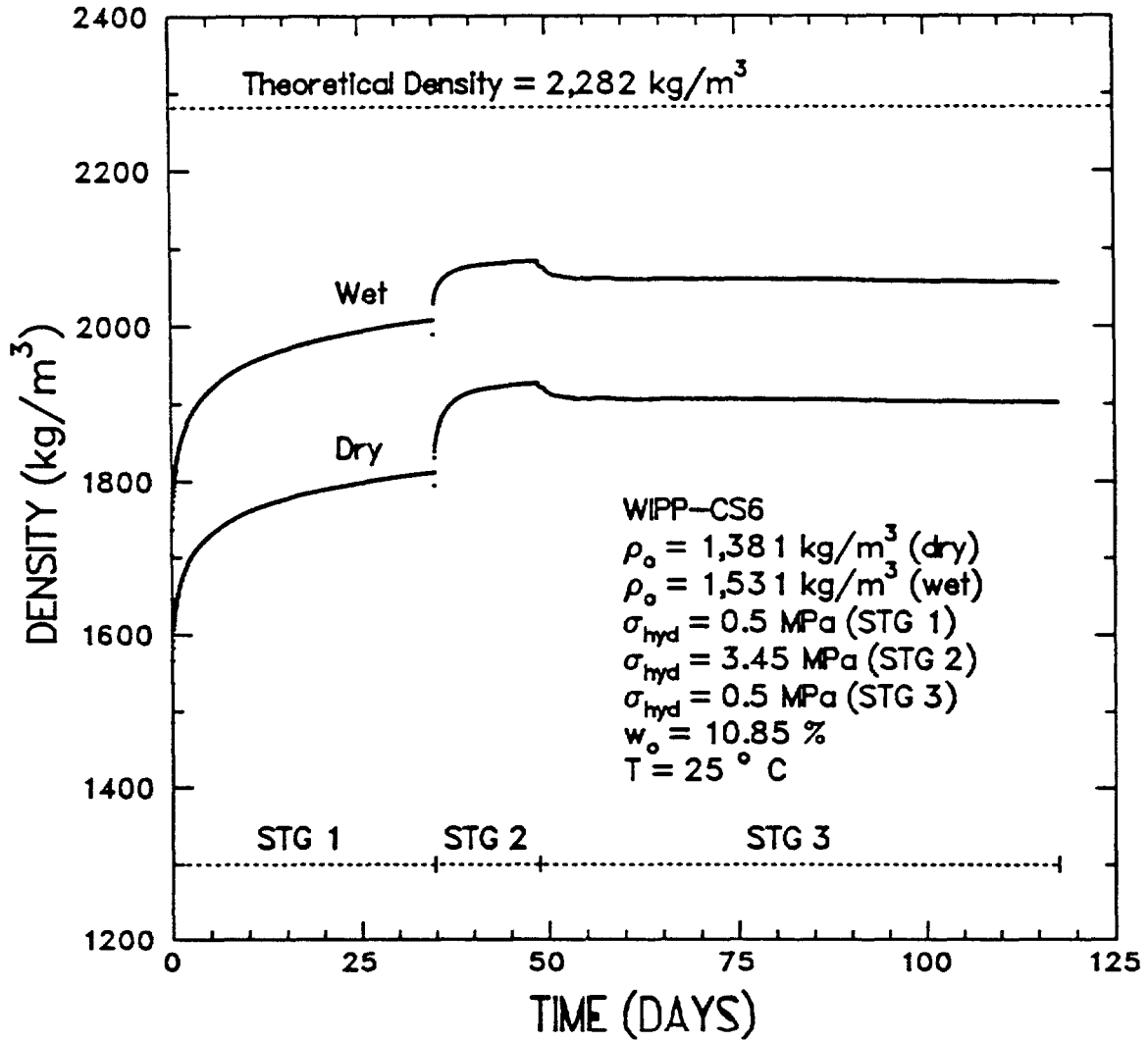


Figure 5-6. Wet and dry density as a function of time for WIPP-CS6, 70/30 crushed salt/bentonite.

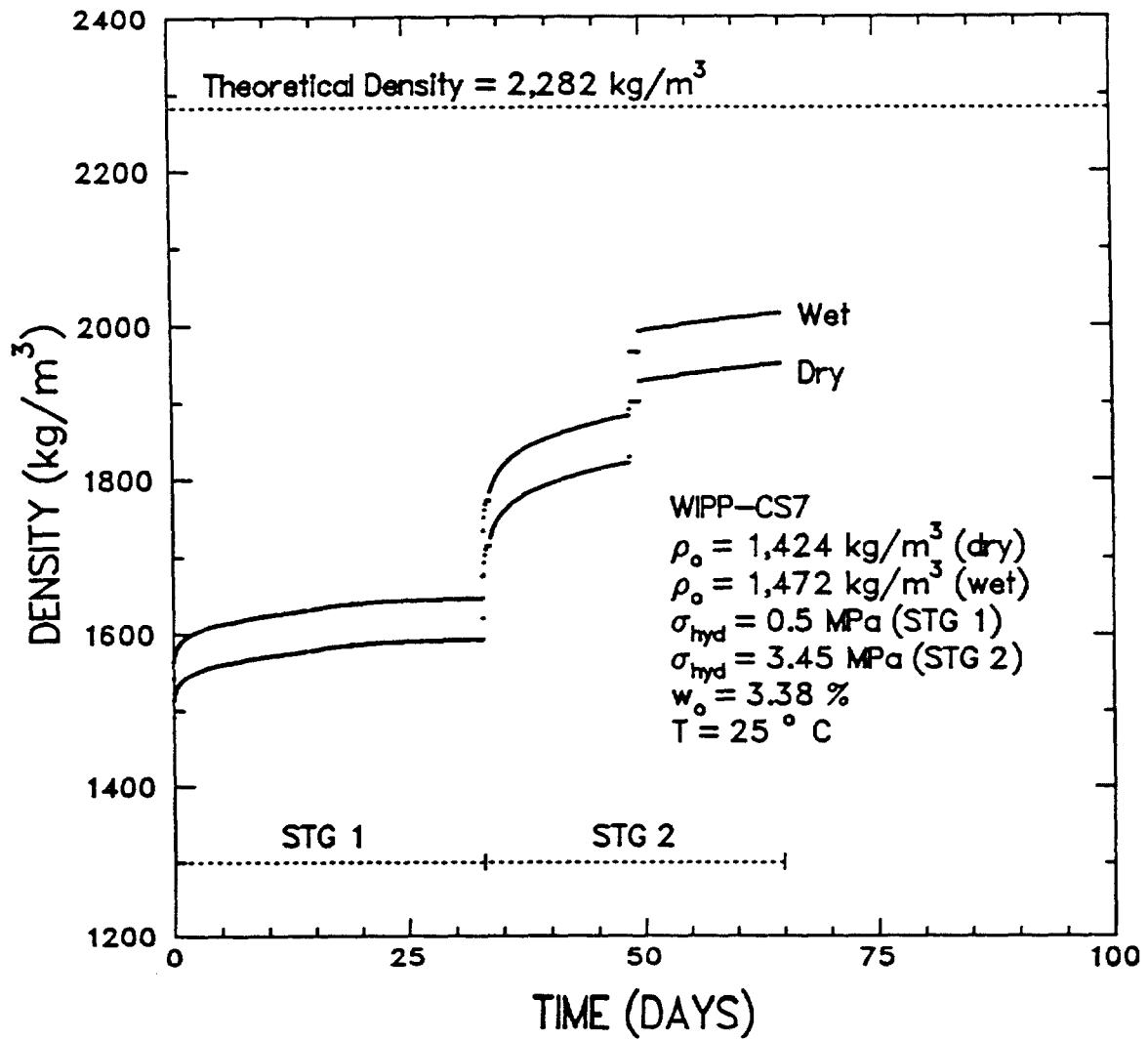


Figure 5-7. Wet and dry density as a function of time for WIPP-CS7, 70/30 crushed salt/bentonite.

5.2 PERMEABILITY

Permeability tests using the steady flow rate of brine method, as described in Section 4.4, were attempted on three of the four specimens and performed successfully on CS6. Permeability measurements were unsuccessful for Test CS5 due to the channeling of brine along the jacket and for Test CS8 because flow was not established. No permeability test was conducted on Test CS7 because it did not reach saturation. The successful test was performed on a saturated specimen at a confining pressure of 0.5 MPa and a pressure drop across the specimen of 345 kPa. The confining pressure for this stage was kept below the pressure used in the previous test stage to prevent continued specimen deformation and also to prevent water from being expelled from the pores of the specimen during the measurement.

Permeability tests were continued until a constant flow rate of brine was established. Permeabilities were calculated from Darcy's law, i.e.,

$$k = \frac{Q}{A} \cdot \frac{\mu L}{\Delta P} \quad (5-5)$$

where

- k = Permeability (having units L^2)
- Q = Measured flow rate of brine (having units L^3T^{-1})
- A = Current area (having units L^2)
- μ = Viscosity of brine (having units $ML^{-1}T^{-1}$)
- L = Current length (having units L)
- ΔP = Pressure drop across specimen (having units $ML^{-1}T^{-2}$)

A viscosity of 1.26 cP ($1.26 \times 10^{-3} \text{kg} \cdot \text{m}^{-1} \cdot \text{s}^{-1}$) was used for brine after Shor et al. [1981]. The flow-versus-time data for CS6 are given in Figure 5-9. The flow rate of 0.089 ml/day was determined from a linear least squares fit to the flow data. Table 5-2 gives permeability as calculated using Equation 5-5. For the durations of the permeability stages imposed, the smallest permeability value that could be determined under these conditions was about $4 \times 10^{-21} \text{m}^2$. The measured permeability for Test CS5 was $1.12 \times 10^{-19} \text{m}^2$, which was slightly lower than expected based on the work of Pfeifle [1991] who found permeabilities to range from $1.3 \times 10^{-18} \text{m}^2$ to $4.9 \times 10^{-18} \text{m}^2$ for WIPP 70/30 crushed salt/bentonite specimens. Pfeifle's data are reproduced in Table 5-2 for comparison. The data show that lower permeabilities correlate with higher density specimens.

5.3 STRENGTH

The strength of the CS5 specimen was determined from an unconfined compression test performed at a constant strain rate of $10^{-5} \cdot \text{s}^{-1}$. Figure 5-10 gives the axial stress-strain curve for this specimen. The unconfined strength was calculated from

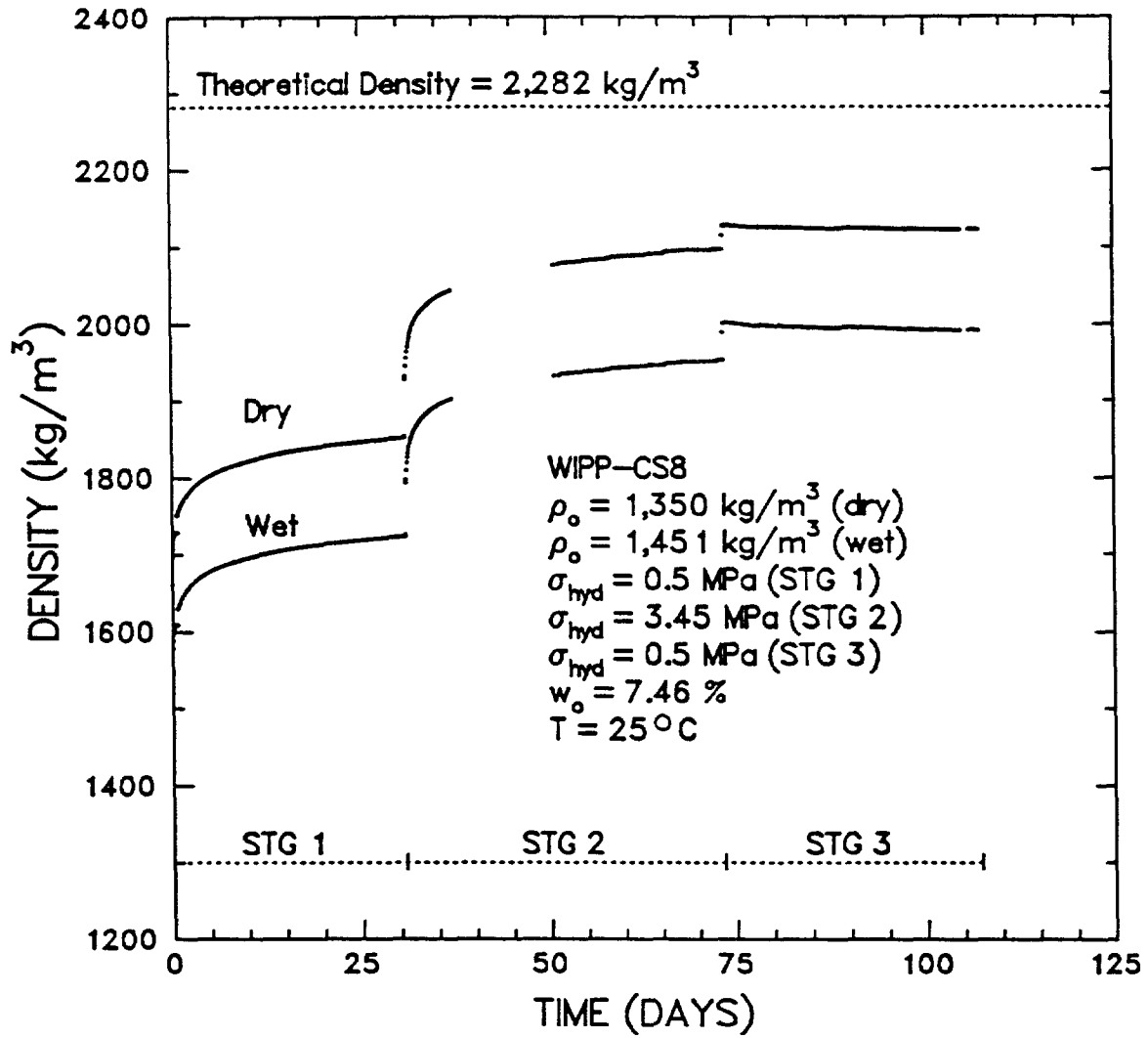


Figure 5-8. Wet and dry density as a function of time for WIPP-CS8, 70/30 crushed salt/bentonite.

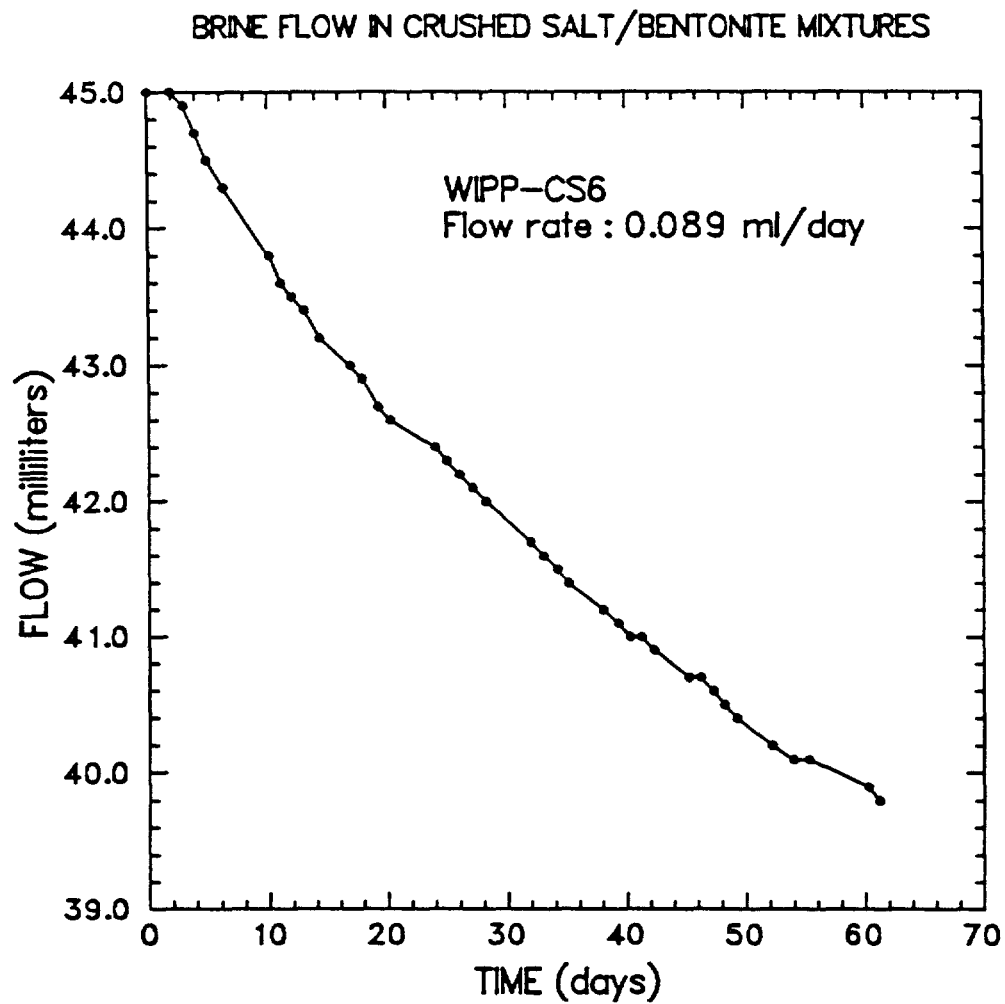


Figure 5-9. Brine flow as a function of time for WIPP-CS6.

$$q_u = \frac{F_{ult}}{A} \quad (5-6)$$

where F_{ult} is the peak or ultimate force sustained by the specimen and A is the original cross-sectional area of the specimen. Table 5-2 also gives the calculated unconfined compressive strength for this specimen and additional data from Pfeifle [1991]. This strength value is consistent with the conclusion of Pfeifle [1991] that higher strengths are measured at higher densities. The strength-versus-density data are shown in Figure 5-11.

Table 5-2. Summary of Permeabilities and Strength

Specimen ID	Water Content Dry Wt. (%)	Final Dry Density (kg m ⁻³)	Permeability (m ² × 10 ⁻¹⁹)	Unconfined Strength (MPa)
CS5	7.47	1,963	(a)	1.66
CS6	10.85	1,956	1.12	—
CS7	3.38	1,858 ^(b)	(b)	—
CS8	7.46	1,927	(c)	—
CS1 ^(d)	5.3	2,034	(e)	8.1
CS3 ^(d)	10.0	1,946	13	1.1
CS4 ^(d)	5.2	1,898	49	0.5

(a) No permeability measurement due to channeling along jacket.

(b) Test terminated after Stage 2.

(c) No flow established after 34 days.

(d) Data from Pfeifle [1991].

(e) No flow established after 167 days.

5.4 WATER CONTENT DISTRIBUTION

The distribution of water content was determined using the method described in Section 4.6 for Specimen CS5. Table 5-3 gives the water contents for the eight samples obtained from the specimen. The sample numbers are ordered with Sample 1 obtained from the bottom of the specimen and Sample 8 from the top of the specimen. The weighted mean water content, w_{mean} , for the specimen is also shown and is calculated as

$$w_{mean} = \frac{\sum M_i^d w_i}{M_{tot}^d} \quad (5-7)$$

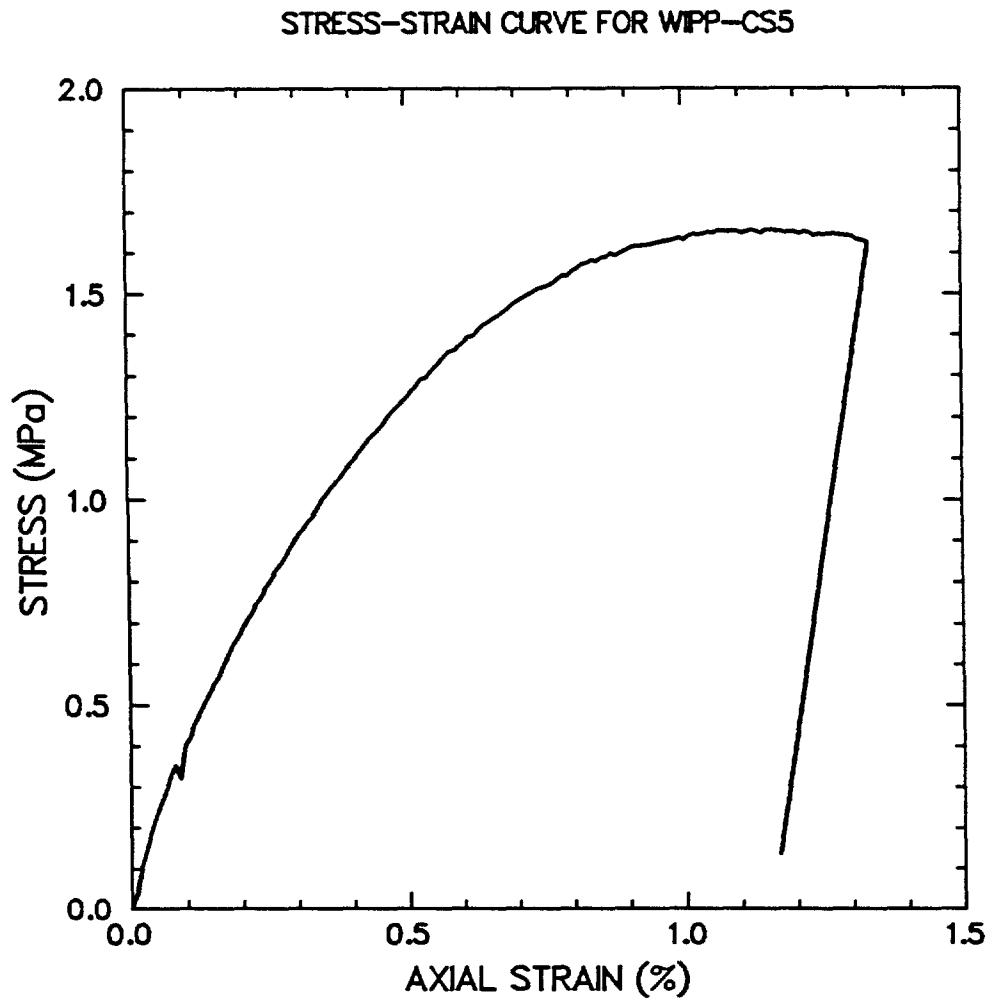


Figure 5-10. Stress-strain curve for unconfined compressive strength test of WIPP-CS5, 70/30 crushed salt/bentonite.

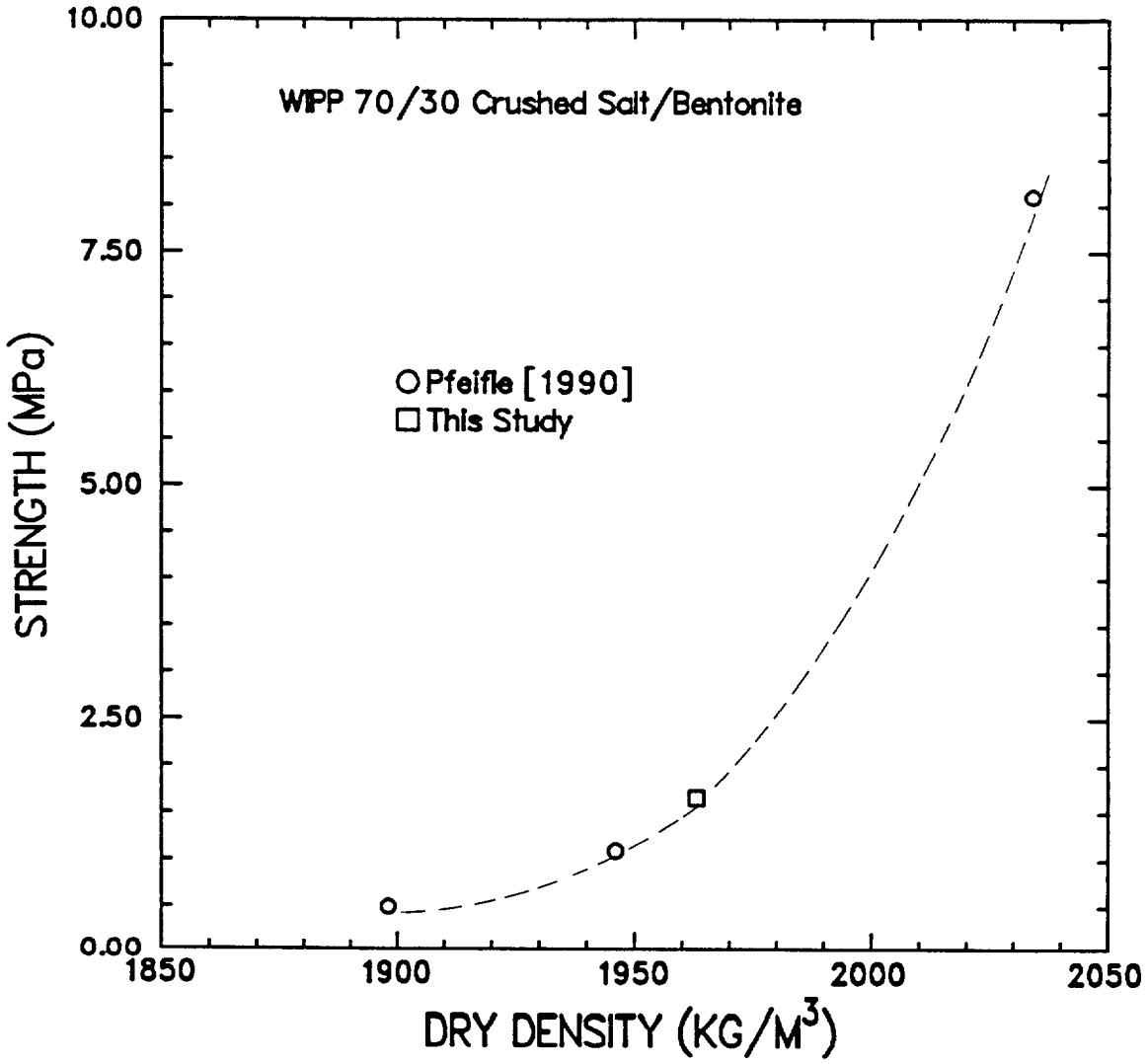


Figure 5-11. Unconfined compressive strength as a function of density for consolidated specimens of WIPP 70/30 crushed salt/bentonite.

where

M^d_i = Dry mass of the i^{th} sample

w_i = Water content of the i^{th} sample expressed as a fraction

M^d_{tot} = Total dry mass

The weighted mean water content for CS5 was 8.09 percent, close to the initial water content for the specimen (7.47 percent). The increase in moisture content is attributed to the permeability test during Stage 3. The water content distribution was generally uniform throughout the specimen except at the ends where it was somewhat higher.

Table 5-3. Water Content Distribution for Test CS5

Specimen ID	Initial Water Content (%)	Sample No.	Dry Mass (g)	Water Content Dry Wt. (%)
CS5	7.47	1	374.26	8.79
		2	255.72	7.98
		3	235.94	7.96
		4	254.60	7.91
		5	264.39	7.65
		6	299.15	7.91
		7	212.76	8.11
		8	297.38	8.15
		Mean ^(a)		

(a) Weighted mean calculated based on dry mass.

6.0 MODEL FITTING

A constitutive model for the consolidation behavior of crushed materials is given by Sjaardema and Krieg [1987]. Their empirical consolidation model is of the form

$$\dot{\rho} = B_0[e^{B_1 P} - 1]e^{A\rho} \quad (6-1)$$

where

$$\begin{aligned} \dot{\rho} &= \text{Time rate of change of density} \\ \rho &= \text{Current density (kg} \cdot \text{m}^{-3}\text{)} \\ P &= \text{Applied pressure (MPa)} \\ B_0, B_1, A &= \text{Fitting parameters} \end{aligned}$$

This equation can be rewritten in terms of the volumetric creep strain rate as:

$$\epsilon_v = \frac{\rho_0}{\rho^2} B_0 [e^{B_1 P} - 1] e^{A\rho} \quad (6-2)$$

where

$$\begin{aligned} \epsilon_v &= \text{Time rate of change of volumetric strain} \\ \rho_0 &= \text{Initial density (kg} \cdot \text{m}^{-3}\text{)} \end{aligned}$$

This equation contains three parameters that must be determined by fitting the model to data. Based on fits made by Pfeifle [1991], Callahan and DeVries [1991] selected values of A , B_0 , and B_1 that are given in Table 6-1. Using these parameter values, predictions of volumetric strain rate as a function of fractional density were made and are shown in comparison with the experimental data in Figures 6-1 through 6-4 for the consolidation stages of Tests CS5, CS6, CS7, and CS8.

For Tests CS5 and CS8, which are at the intermediate moisture contents, the model fits the data for Stage 1 reasonably well. The model overestimates the consolidation rate for Stage 1 of the lower moisture content test (CS7) and underestimates the consolidation rate for the higher moisture content test (CS6). The model underestimates the consolidation rates for Stage 2 in all cases.

Following the method of Pfeifle [1991], the data obtained in this study were also used to fit the Sjaardema and Krieg [1987] model. Equation 6-1 was integrated to express density as a function of time for use in fitting the dry density-time data. Therefore, the model used in the fitting procedure was

$$\rho = -\frac{1}{A} \ln[e^{-A\rho_0} - A \cdot B_0[e^{B_1 P} - 1]t] \quad (6-3)$$

where t is time, in seconds.

Because Equation 6-3 is nonlinear in its parameters, a numerical procedure for solving simultaneous nonlinear equations was employed to minimize the sum-of-squared error defined as

$$S = \sum_{i=1}^n (\rho_i - \hat{\rho}_i)^2 \quad (6-4)$$

where

- n = Total number of measurements in the database
- ρ_i = Measured density at i
- $\hat{\rho}_i$ = Predicted density at i from Equation 6-3

In solving the nonlinear equations that arise from minimizing S , linear approximations to the equations were used. The parameter values determined by Callahan and DeVries [1991] were used as initial estimates of the unknown parameters and were used to evaluate the coefficients in the linearized system of equations. The system of equations was solved to obtain new estimates of the parameters, and the process was repeated until S was minimized. The numerical procedure employed in solving the equations was the Gauss/Newton method [Hartley, 1961].

Because the original databases contained large numbers of measurements (>5,000), a new database was derived before the fitting procedure was employed. The new database included 100 measurements (equally spaced in time) from the first two stages of each test, and therefore contained 800 measurements. No measurements from the permeability stages were included in the databases. This approach was used so that the model parameters would be sensitive to changes in pressure and initial density, as well as time.

Table 6-1 gives the parameter values determined from the fit. The values of A and B_0 changed very little, 4 and 20 percent, respectively. The value of B_1 , the parameter that controls the sensitivity of consolidation rate to pressure, changed by approximately a factor of 3. The parameters used by Callahan and DeVries [1991] were based on data obtained at pressures of 3.45 MPa, 7 MPa, and 15 MPa; whereas in this study, pressures of 0.5 MPa and 3.45 MPa were used. The increase in the value of B_1 might therefore be a result of fitting the model to lower pressures.

The model predictions of volumetric strain rate will, of course, change with the new parameter values. The model predictions obtained with different sets of parameter values are compared in Figures 6-5 and 6-6 for pressures of 0.05 MPa and 15 MPa, respectively. Parameter values given by Sjaardema and Krieg [1987] for crushed salt, and by Callahan and DeVries [1991] and this study for a crushed

salt/bentonite mixture are shown. The curves for the crushed salt/bentonite mixture were calculated based on an intact density of $2,260 \text{ kg}\cdot\text{m}^{-3}$ since that value was used by Callahan and DeVries [1991]. The predicted slopes for the mixture are essentially the same; the change in B_1 causes the predicted curves to be offset from one another.

The new parameter values obtained in this study were input into the Sjaardema and Krieg [1987] model, and the new predicted consolidation rates were plotted along with the experimental data in Figures 6-7 through 6-10 for the four tests. Since the model is now fitted solely to the data of this study, an improved fit is expected. The fit is improved at both pressures for Tests CS5 and CS7; however, for Tests CS6 and CS8, the fit is improved for data at 3.45 MPa but worse for data at 0.5 MPa.

Table 6-1. Parameter Values for Density Model

Test Data	Parameter Values ^(a)		
	A ($\text{m}^3 \cdot \text{kg}^{-1} \times 10^{-3}$)	B_0 ($\text{kg} \cdot \text{m}^{-3} \cdot \text{s}^{-1} \times 10^{21}$)	B_1 (MPa^{-1})
Callahan and DeVries [1990]	-34.5	1.000	.600
This Study	-36.0	1.201	1.845

$$(a) \quad \rho = -\frac{1}{A} \ln \left\{ e^{-A\rho_0} - AB_0 \left[e^{B_1 P} - 1 \right] t \right\}$$

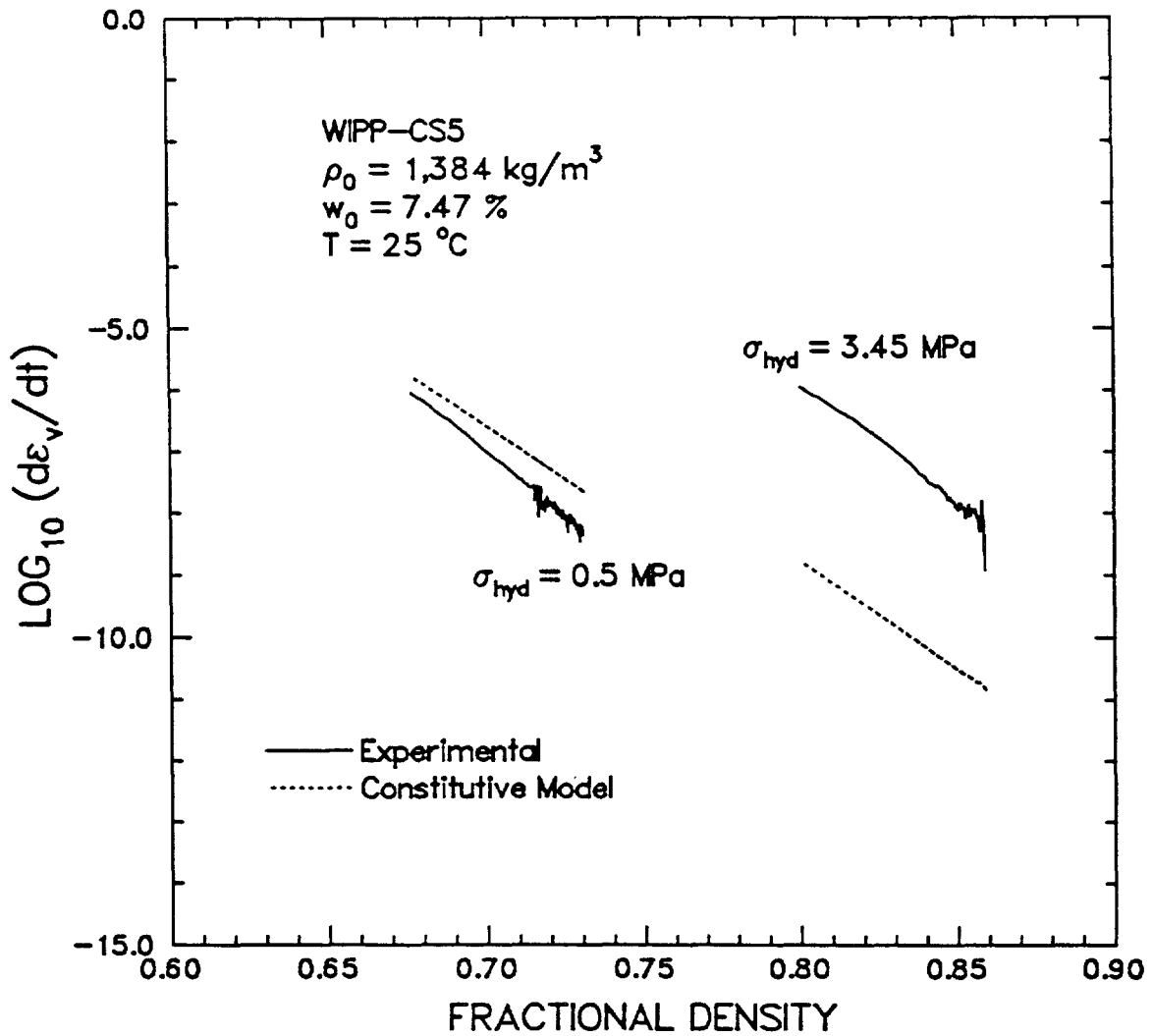


Figure 6-1. Log₁₀ volumetric strain rate-versus-fractional density for WIPP-CS5, 70/30 crushed salt/bentonite, and prediction based on Sjaardema and Krieg [1987] constitutive model with parameters fit by Callahan and DeVries [1991].

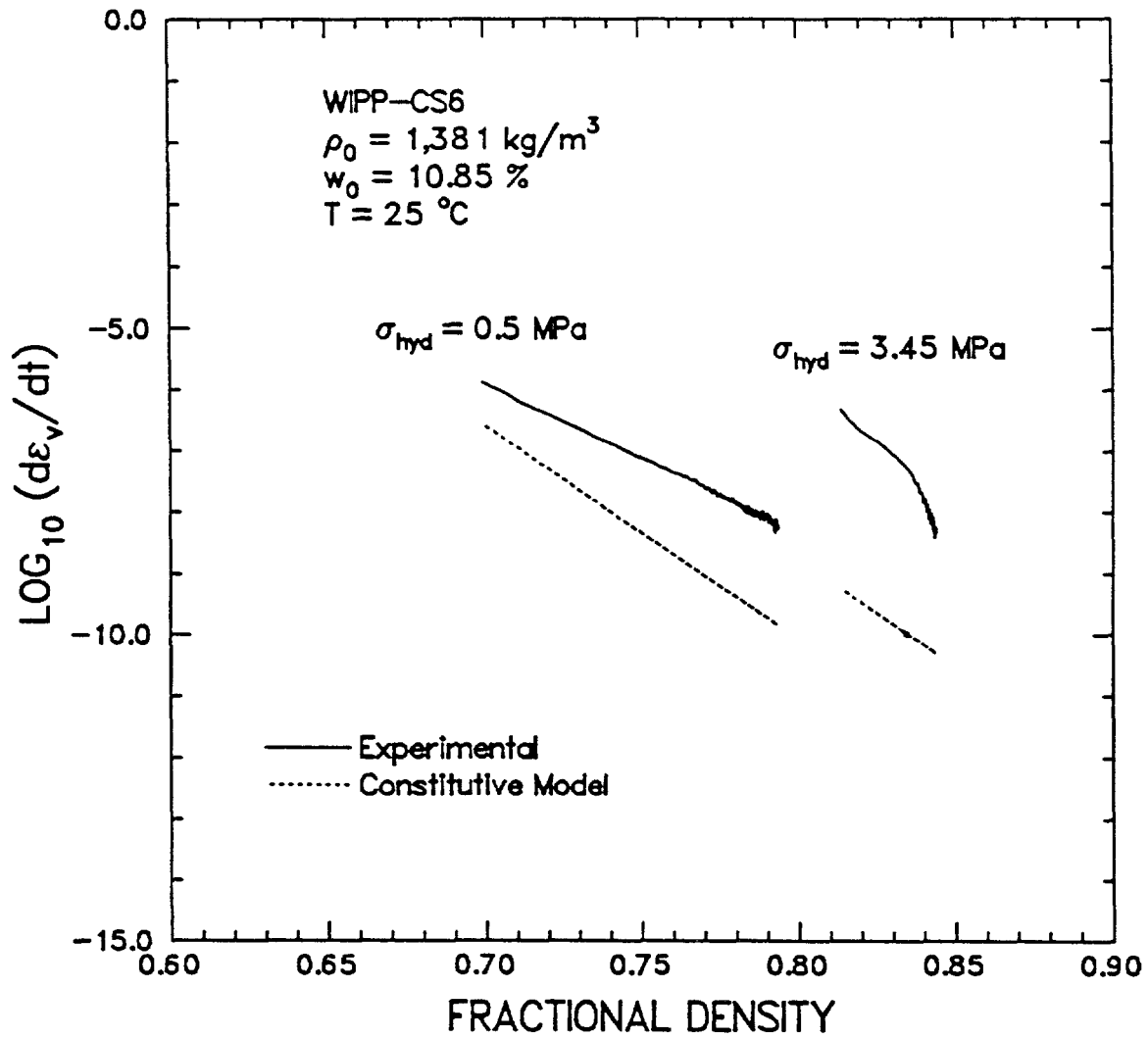


Figure 6-2. Log₁₀ volumetric strain rate-versus-fractional density for WIPP-CS6, 70/30 crushed salt/bentonite, and prediction based on Sjaardema and Krieg [1987] constitutive model with parameters fit by Callahan and DeVries [1991].

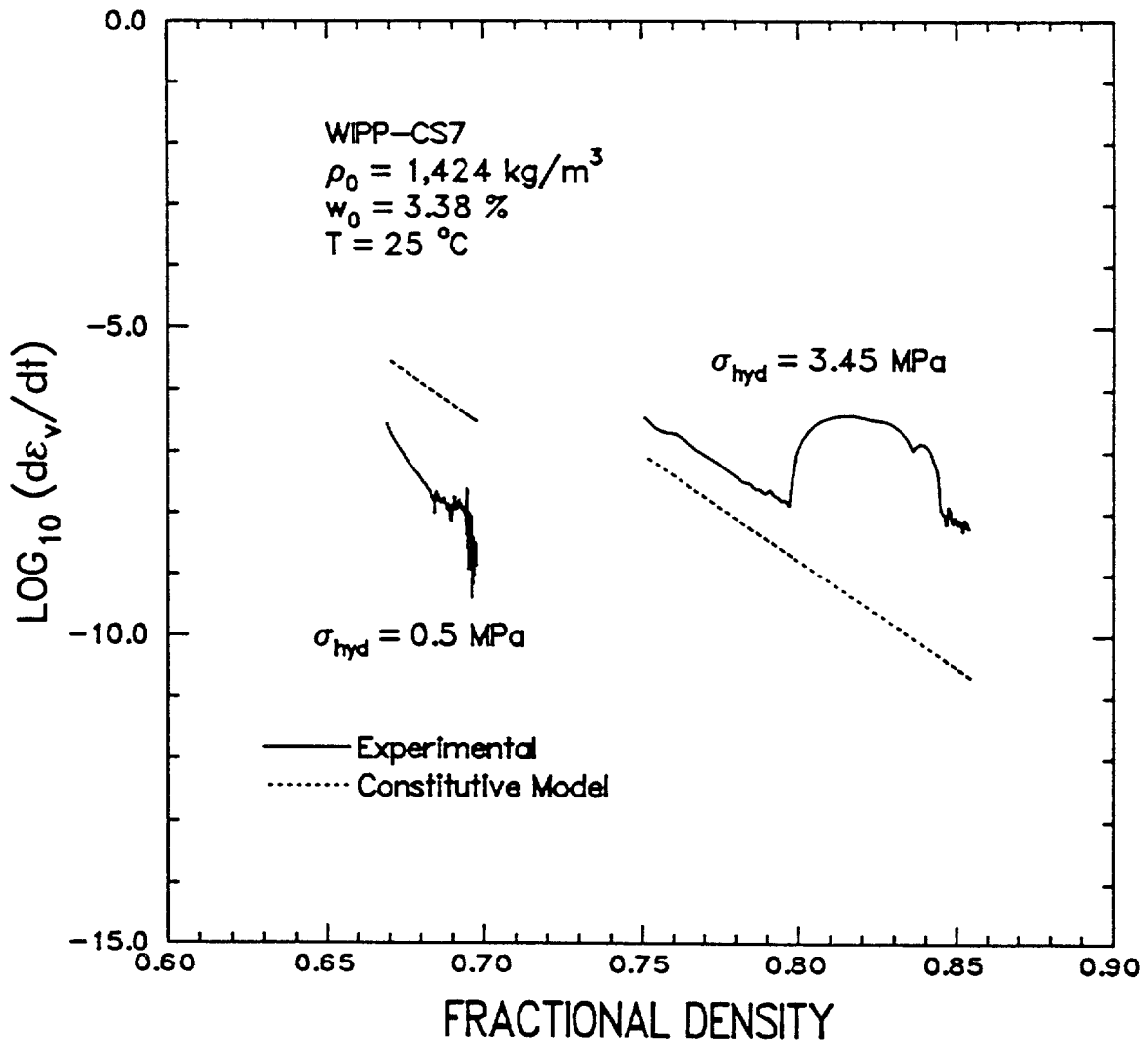


Figure 6-3. Log₁₀ volumetric strain rate-versus-fractional density for WIPP-CS7, 70/30 crushed salt/bentonite, and prediction based on Sjaardema and Krieg [1987] constitutive model with parameters fit by Callahan and DeVries [1991].

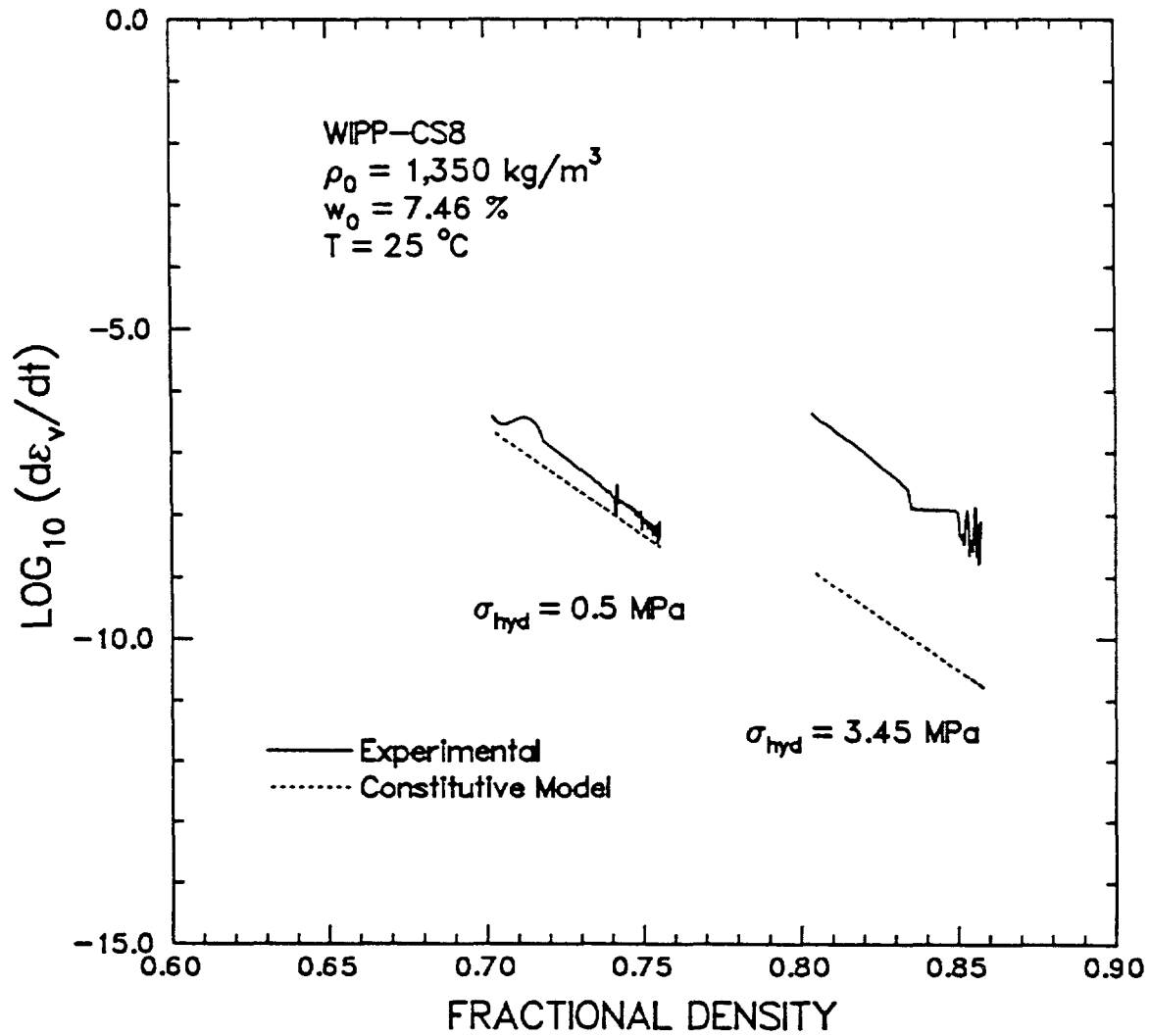


Figure 6-4. Log₁₀ volumetric strain rate-versus-fractional density for WIPP-CS8, 70/30 crushed salt/bentonite, and prediction based on Sjaardema and Krieg [1987] constitutive model with parameters fit by Callahan and DeVries [1991].

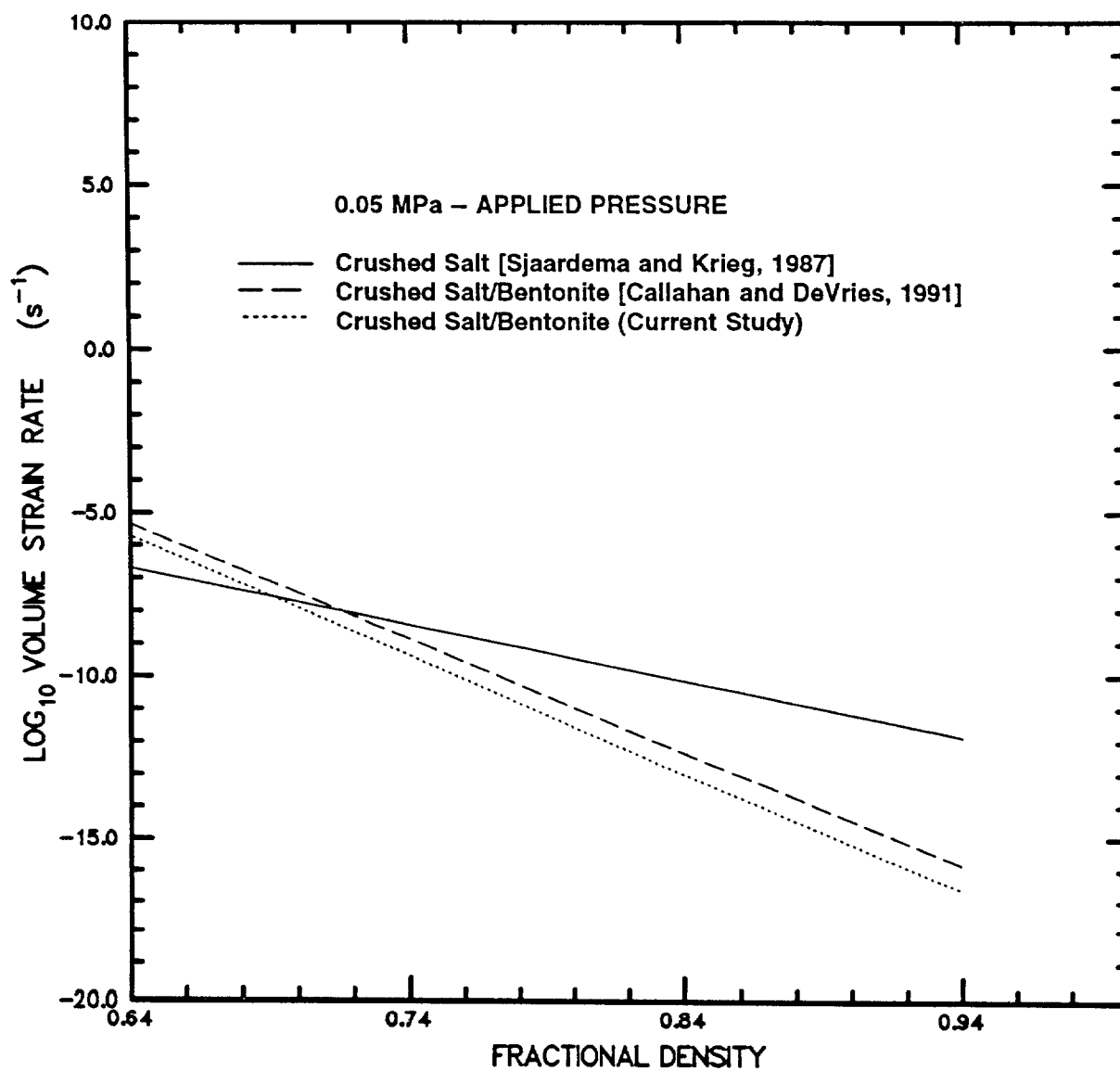


Figure 6-5. A comparison of three sets of parameter values used in the Sjaardema and Krieg [1987] constitutive model at 0.05 MPa pressure.

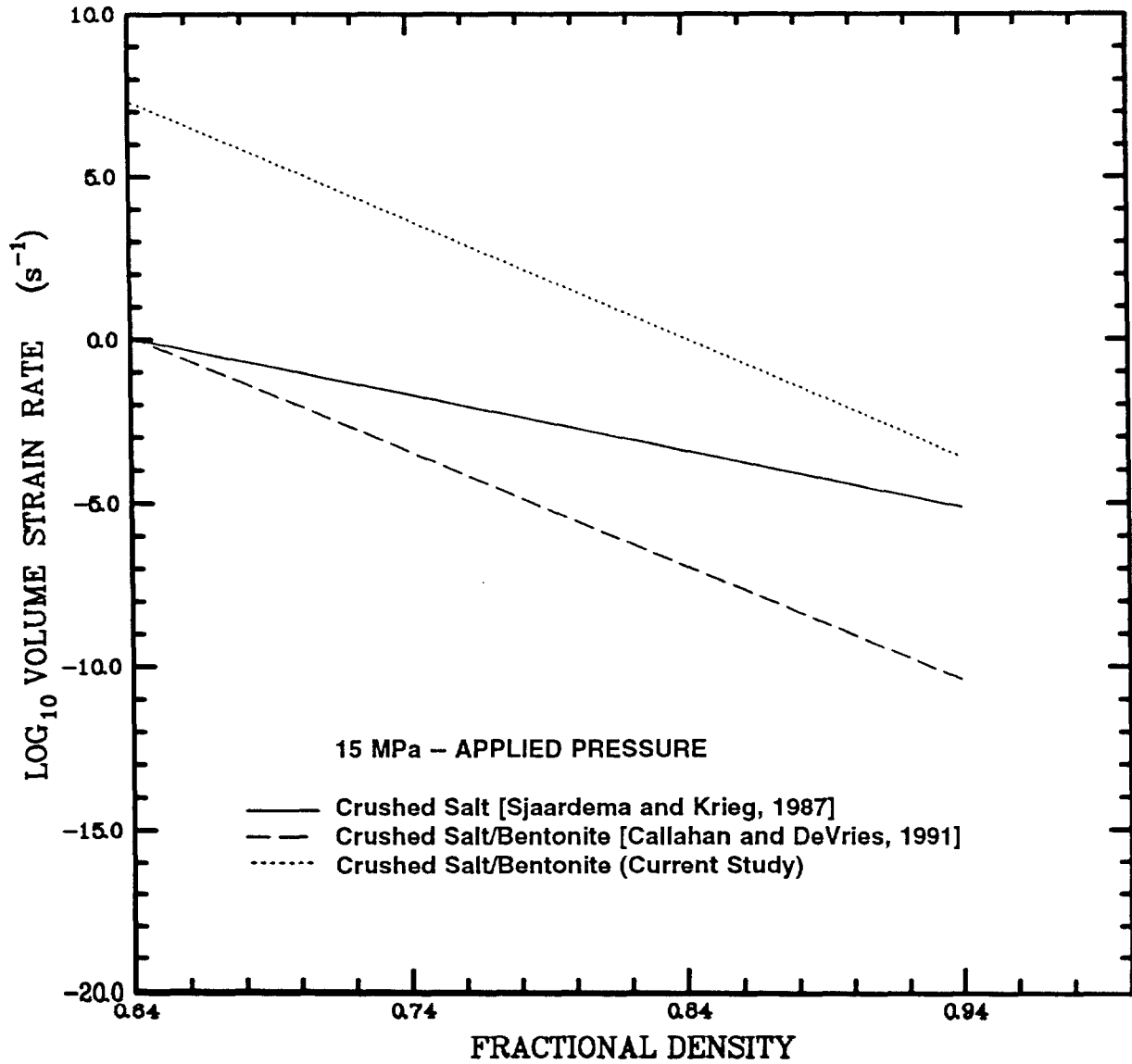


Figure 6-6. A comparison of three sets of parameter values used in the Sjaardema and Krieg [1987] constitutive model at 15 MPa pressure.

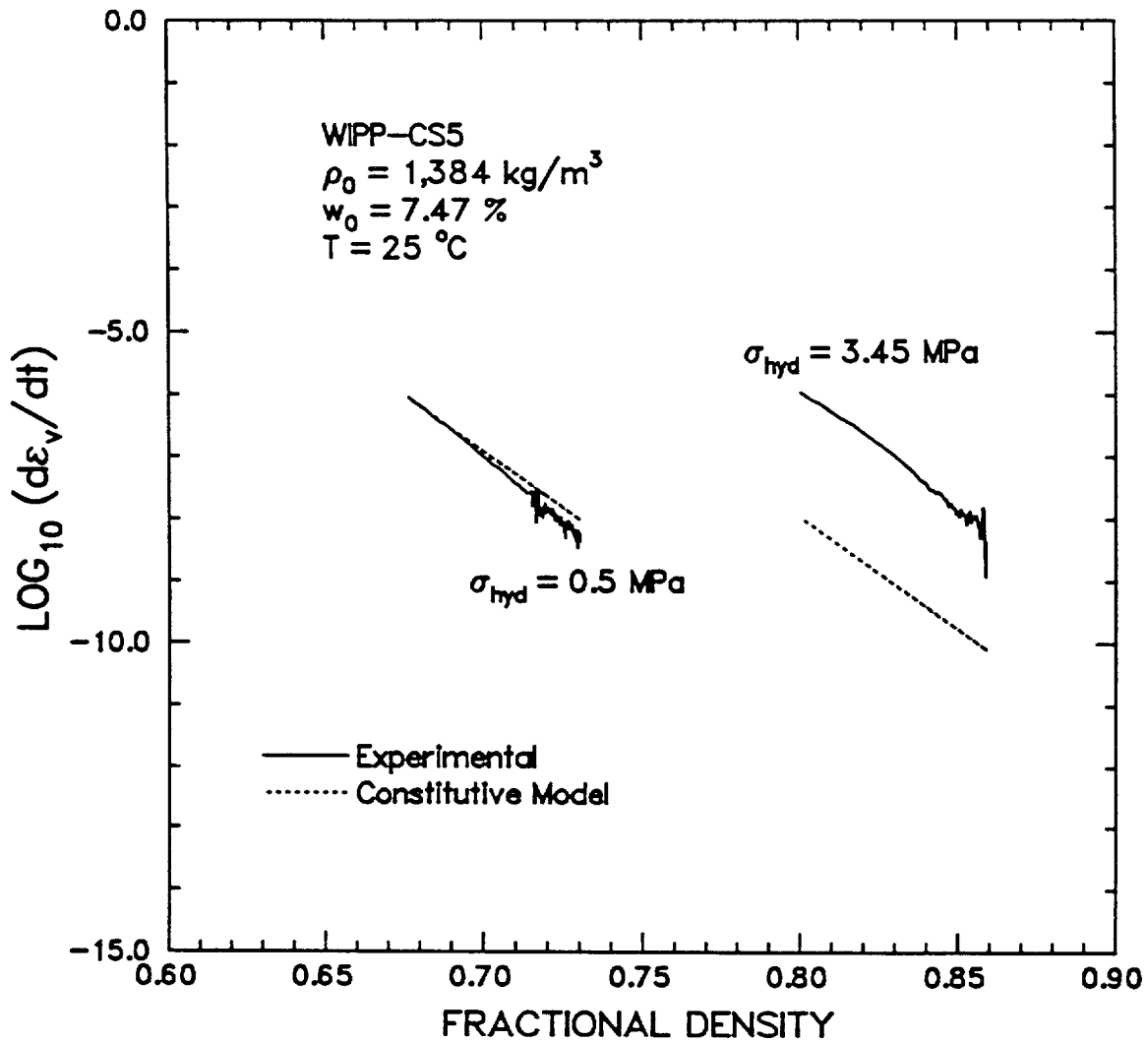


Figure 6-7. Log₁₀ volumetric strain rate-versus-fractional density for WIPP-CS5, 70/30 crushed salt/bentonite and prediction based on Sjaardema and Krieg [1987] constitutive model with parameters fit in this study.

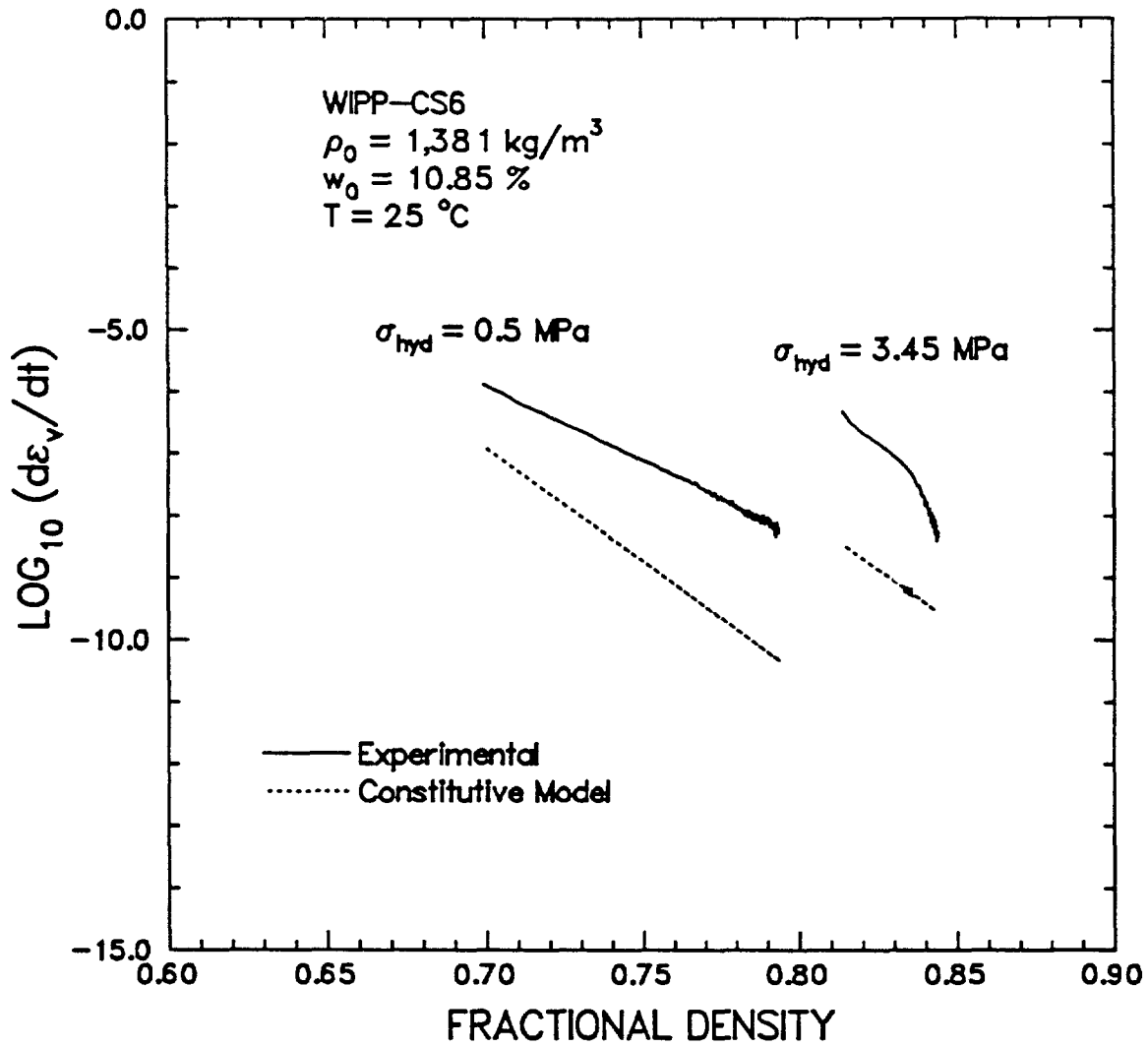


Figure 6-8. Log₁₀ volumetric strain rate-versus-fractional density for WIPP-CS6, 70/30 crushed salt/bentonite and prediction based on Sjaardema and Krieg [1987] constitutive model with parameters fit in this study.

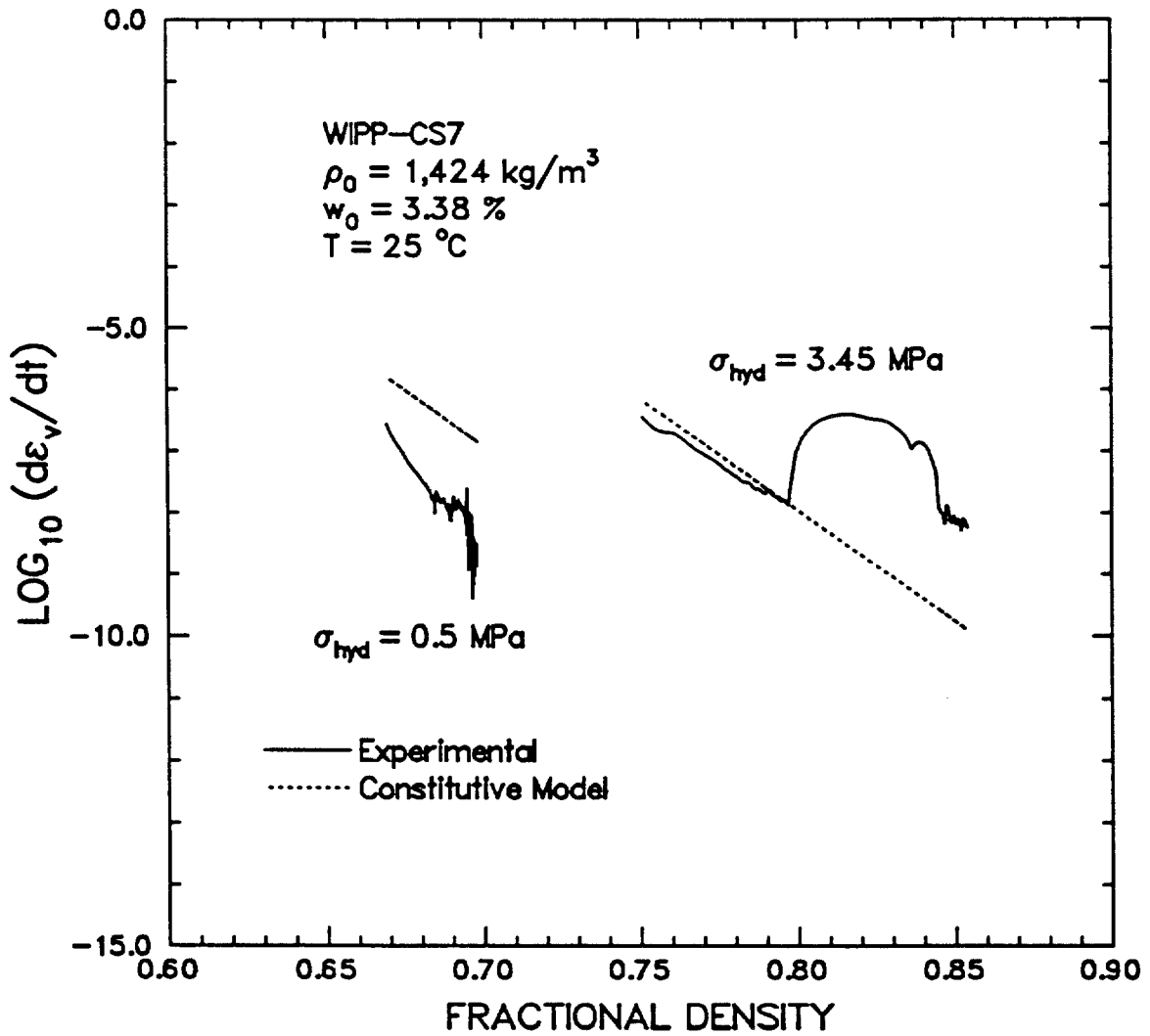


Figure 6-9. Log₁₀ volumetric strain rate-versus-fractional density for WIPP-CS7, 70/30 crushed salt/bentonite and prediction based on Sjaardema and Krieg [1987] constitutive model with parameters fit in this study.

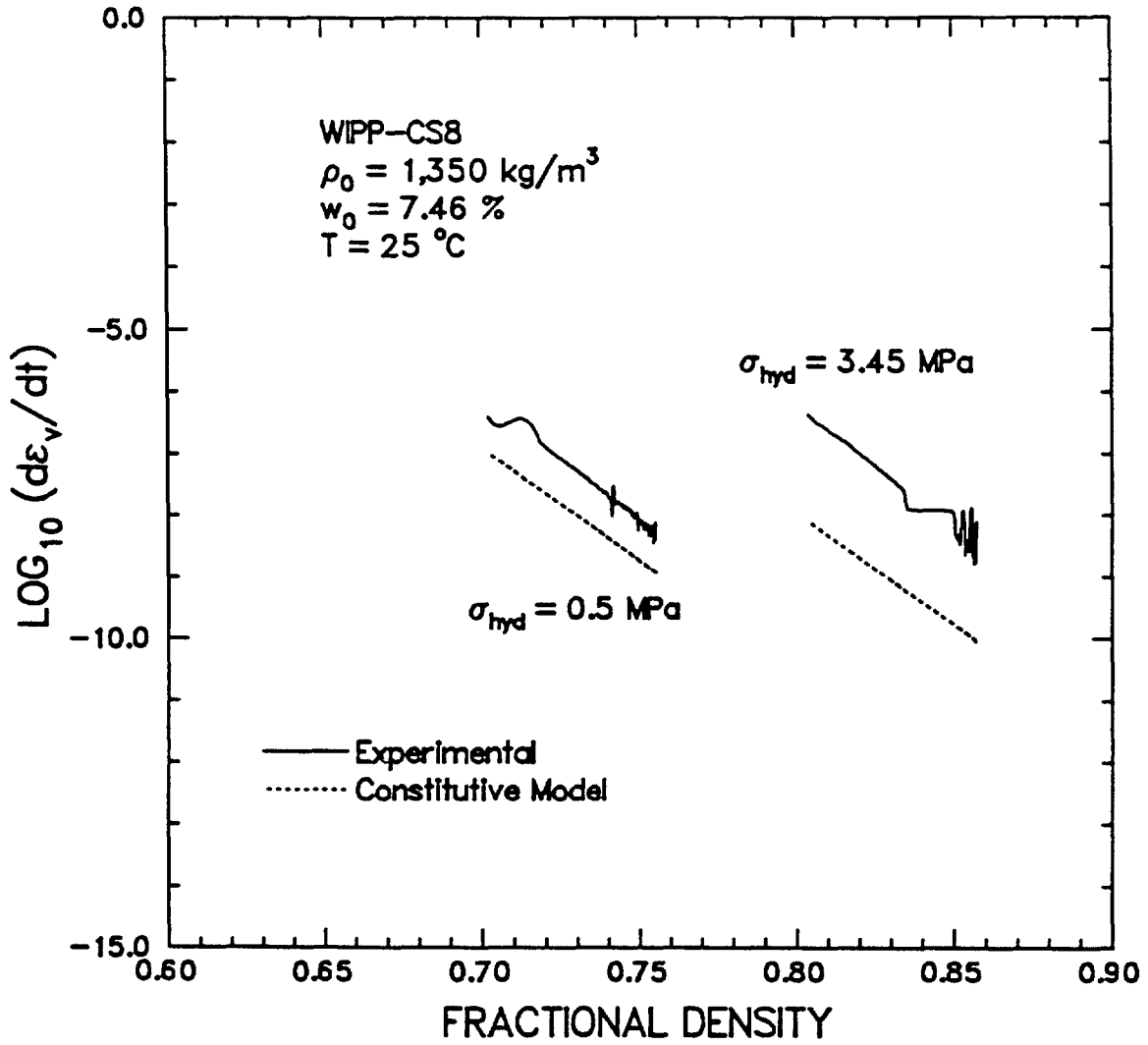


Figure 6-10. Log₁₀ volumetric strain rate-versus-fractional density for WIPP-CS8, 70/30 crushed salt/bentonite and prediction based on Sjaardema and Krieg [1987] constitutive model with parameters fit in this study.

7.0 SUMMARY AND CONCLUSIONS

Four consolidation tests were performed on specimens of 70 percent crushed salt by dry weight and 30 percent bentonite by dry weight. The specimens were prepared at nominal water contents of 3.5, 7, and 10 percent based on total dry weight. Each test had several stages in which various pressure levels were applied. Stage 1 was at a hydrostatic stress of 0.5 MPa, Stage 2 at 3.45 MPa, and Stage 3, the permeability stage, was at 0.5 MPa. Pressures were maintained until the specimens reached full saturation at which time permeability tests were performed using the constant rate of flow of brine technique. Strength and water content distribution were determined for the CS5 test specimen.

Three of the four specimens reached full saturation after less than 60 days at pressure. A density model proposed by Sjaardema and Krieg [1987] was compared to the dry density data using parameter values established by Callahan and DeVries [1991]. The Sjaardema and Krieg model fit the data best at intermediate moisture contents and during Stage 1 at 0.5 MPa. For Stage 1, the model overestimated the consolidation rate of the lower moisture content test and underestimated the consolidation rate for the higher moisture content test. The model consistently underestimated consolidation rates during Stage 2 at 3.45 MPa. The model was also fitted to the data obtained in this study to determine additional parameter values. Of the three fitting parameters, the parameter that describes the sensitivity of consolidation rate to pressure changed the most substantially.

A constant rate of flow test was successfully performed for one test, and it showed a permeability of $1.12 \times 10^{-19} \text{m}^2$. This is slightly lower than expected based on the results of Pfeifle [1991] who determined a range of permeabilities for saturated specimens of 70/30 crushed salt/bentonite of $1.3 \times 10^{-18} \text{m}^2$ to $4.9 \times 10^{-18} \text{m}^2$. The permeability data show that higher density specimens tend to have lower permeabilities.

The constant strain rate unconfined compressive strength of the CS5 test specimen was 1.66 MPa. This strength, when compared with other data obtained by Pfeifle [1991], is consistent with the conclusion that higher density specimens have higher strengths.

8.0 REFERENCES

Butcher, B.M., C.F. Novak, and M. Jercinovic. 1991. *The Advantages of a Salt/Bentonite Backfill for Waste Isolation Pilot Plant Disposal Rooms*. SAND90-3074. Albuquerque, NM: Sandia National Laboratories.

Callahan G.D., and K.L. DeVries. 1991. *Analyses of Backfilled Transuranic Wastes Disposal Rooms*. SAND91-7052. Albuquerque, NM: Sandia National Laboratories.

Hartley, H.O.. 1961. "The Modified Gauss-Newton Method for Fitting of Non-linear Regression Functions by Least Squares," *Technometrics*. Vol. 3, 269-280.

Holcomb, D.J., and D.W. Hannum. 1982. *Consolidation of Crushed Salt Backfill Under Conditions Appropriate to the WIPP Facility*. SAND82-0630. Albuquerque, NM: Sandia National Laboratories.

Pfeifle, T.W. 1987. *Backfill Material Specifications and Requirements for the WIPP Simulated DHLW and TRU Waste Technology Experiments*. SAND85-7209. Albuquerque, NM: Sandia National Laboratories.

Pfeifle, T.W., 1991. *Consolidation, Permeability, and Strength of Crushed Salt/Bentonite With Application to the WIPP*. SAND90-7009. Albuquerque, NM: Sandia National Laboratories.

Pfeifle, T.W., and P.E. Senseny. 1985. *Permeability and Consolidation of Crushed Salt From the WIPP Site*. Topical Report RSI-0278. Rapid City, SD: RE/SPEC Inc.

Shor, A.J., C.F. Baes, Jr., and C.M. Canonico. 1981. *Consolidation and Permeability of Salt in Brine*. ORNL-5774. Oak Ridge, TN: Oak Ridge National Laboratory.

Sjaardema, G.D., and R.D. Krieg. 1987. *A Constitutive Model for the Consolidation of WIPP Crushed Salt and Its Use in Analyses of Backfilled Shaft and Drift Configurations*. SAND87-1977. Albuquerque, NM: Sandia National Laboratories.

Stroup, D.E., and P.E. Senseny. 1987. *Influence of Bentonite Content on Consolidation and Permeability of Crushed Salt From the WIPP*. Topical Report RSI-0309. Rapid City, SD: RE/SPEC Inc.

DISTRIBUTION

Federal Agencies

US Department of Energy, (5)
Office of Civilian Radioactive Waste
Management

Attn: Deputy Director, RW-2
Associate Director, RW-10
Office of Program
Administration and
Resources Management
Associate Director, RW-20
Office of Facilities
Siting and Development
Associate Director, RW-30
Office of Systems
Integration and
Regulations
Associate Director, RW-40
Office of External
Relations and Policy
Forrestal Building
Washington, DC 20585

US Department of Energy (4)
WIPP Project Integration Office
Attn: W.J. Arthur III
L.W. Gage
P.J. Higgins
D.A. Olona
PO Box 5400
Albuquerque, NM 87115-5400

US Department of Energy
Attn: National Atomic Museum Library
Albuquerque Operations Office
PO Box 5400
Albuquerque, NM 87185-5400

US Department of Energy (4)
WIPP Project Site Office (Carlsbad)
Attn: R. Becker
V. Daub
J. Lippis
J.A. Mewhinney
PO Box 3090
Carlsbad, NM 88221

US Department of Energy
Research & Waste Management Division
Attn: Director
PO Box E
Oak Ridge, TN 37831

US Department of Energy
Attn: E. Young
Room E-178
GAO/RCED/GTN
Washington, DC 20545

US Department of Energy
Office of Environmental Restoration
and Waste Management
Attn: J. Lytle, EM-30 (Trevion II)
Washington, DC 20585-0002

US Department of Energy (3)
Office of Environmental Restoration
and Waste Management
Attn: M. Frei, EM-34 (Trevion II)
Washington, DC 20585-0002

US Department of Energy
Office of Environmental Restoration
and Waste Management
Attn: S. Schneider, EM-342
(Trevion II)
Washington, DC 20585-0002

US Department of Energy (3)
Office of Environment, Safety
and Health
Attn: C. Borgstrom, EH-25
R. Pelletier, EH-231
Washington, DC 20585

US Department of Energy (2)
Idaho Operations Office
Fuel Processing and Waste
Management Division
785 DOE Place
Idaho Falls, ID 83402

US Environmental Protection
Agency (2)
Radiation Programs (ANR-460)
Attn: R. Guimond
Washington, DC 20460

US Geological Survey (2)
Water Resources Division
Attn: R. Livingston
Suite 200
4501 Indian School, NE
Albuquerque, NM 87110

US Nuclear Regulatory Commission
Attn: H. Marson
Mail Stop 623SS
Washington, DC 20555

NM Environment Department
WIPP Project Site
Attn: P. McCasland
PO Box 3090
Carlsbad, NM 88221

Boards

Defense Nuclear Facilities Safety
Board
Attn: D. Winters
Suite 700
625 Indiana Ave., NW
Washington, DC 20004

Nuclear Waste Technical Review
Board (2)
Attn: D.A. Deere
S.J.S. Parry
Suite 910
1100 Wilson Blvd.
Arlington, VA 22209-2297

Advisory Committee on Nuclear Waste
Nuclear Regulatory Commission
Attn: R. Major
7920 Norfolk Ave.
Bethesda, MD 20814

State Agencies

Environmental Evaluation Group (3)
Attn: Library
Suite F-2
7007 Wyoming, NE
Albuquerque, NM 87109

NM Bureau of Mines and Mineral
Resources
Socorro, NM 87801

NM Energy, Minerals, and Natural
Resources Department
Attn: Library
2040 S. Pacheco
Santa Fe, NM 87505

NM Environment Department (3)
Secretary of the Environment
Attn: J. Espinosa
1190 St. Francis Drive
Santa Fe, NM 87503-0968

Laboratories/Corporations

Battelle Pacific Northwest
Laboratories (2)
Attn: H.C. Burkholder, P7-41
R.E. Westerman, P8-37
Battelle Blvd.
Richland, WA 99352

Savannah River Laboratory (3)
Attn: N. Bibler
M.J. Plodinec
G.G. Wicks
Aiken, SC 29801

INTERA Inc.
Attn: J.F. Pickens
Suite 300
6850 Austin Center Blvd.
Austin, TX 78731

INTERA Inc.
Attn: W. Stensrud
PO Box 2123
Carlsbad, NM 88221

IT Corporation
Attn: R.F. McKinney
Regional Office - Suite 700
5301 Central, NE
Albuquerque, NM 87108

Los Alamos National Laboratory
Attn: B. Erdal, CNC-11
PO Box 1663
Los Alamos, NM 87544

RE/SPEC, Inc.
Attn: W. Coons
Suite 300
4775 Indian School, NE
Albuquerque, NM 87110-3927

RE/SPEC, Inc. (8)
Attn: N. Brodsky (5)
G. Callahan
T. Pfeifle
L. Ratigan
PO Box 725
Rapid City, SD 57709

Southwest Research Institute (2)
Center for Nuclear Waste
Regulatory Analysis
Attn: P.K. Nair
6220 Culebra Road
San Antonio, TX 78228-0510

SAIC
Attn: G. Dymmel
101 Convention Center Dr.
Las Vegas, NV 89109

SAIC
Attn: H.R. Pratt,
10260 Campus Point Dr.
San Diego, CA 92121

SAIC (2)
Attn: M. Davis
J. Tollison
2109 Air Park Rd., SE
Albuquerque, NM 87106

Tech Reps Inc. (3)
Attn: J. Chapman
R. Jones
E. Lorusso
5000 Marble, NE
Albuquerque, NM 87110

Westinghouse Electric Corporation (5)
Attn: Library
C. Cox
L. Fitch
R. Kehrman
L. Trego
PO Box 2078
Carlsbad, NM 88221

Universities

University of New Mexico
Geology Department
Attn: Library
Albuquerque, NM 87131

University of Washington
Attn: G.R. Heath
College of Ocean
and Fishery Sciences
583 Henderson Hall
Seattle, WA 98195

Individuals

P. Drez
8816 Cherry Hills Rd., NE
Albuquerque, NM 87111

D.W. Powers
Star Route Box 87
Anthony, TX 79821

Libraries

Thomas Brannigan Library
Attn: D. Dresp
106 W. Hadley St.
Las Cruces, NM 88001

Hobbs Public Library
Attn: M. Lewis
509 N. Ship St.
Hobbs, NM 88248

New Mexico State Library
Attn: N. McCallan
325 Don Gaspar
Santa Fe, NM 87503

New Mexico Tech
Martin Speere Memorial Library
Campus Street
Socorro, NM 87810

New Mexico Junior College
Pannell Library
Attn: R. Hill
Lovington Highway
Hobbs, NM 88240

WIPP Public Reading Room
Carlsbad Public Library
Attn: Director
101 S. Halagueno St.
Carlsbad, NM 88220

Government Publications Department
General Library
University of New Mexico
Albuquerque, NM 87131

**National Academy of Sciences,
WIPP Panel**

Charles Fairhurst, Chairman
Department of Civil and
Mineral Engineering
University of Minnesota
500 Pillsbury Dr., SE
Minneapolis, MN 55455-0220

Howard Adler
Oak Ridge Associated Universities
Medical Sciences Division
PO Box 117
Oak Ridge, TN 37831-0117

John D. Bredehoeft
Western Region Hydrologist
Water Resources Division
US Geological Survey (M/S 439)
345 Middlefield Road
Menlo Park, CA 94025

Fred M. Ernsberger
250 Old Mill Road
Pittsburgh, PA 15238

Rodney C. Ewing
Department of Geology
University of New Mexico
Albuquerque, NM 87131

B. John Garrick
PLG, Inc.
Suite 400
4590 MacArthur Blvd.
Newport Beach, CA 92660-2027

Leonard F. Konikow
US Geological Survey
431 National Center
Reston, VA 22092

Jeremiah O'Driscoll
Jody Incorporated
505 Valley Hill Drive
Atlanta, GA 30350

Christopher G. Whipple
Clement International
Suite 1380
160 Spear St.
San Francisco, CA 94105

Peter B. Myers
National Academy of Sciences
Board on Radioactive
Waste Management
2101 Constitution Ave.
Washington, DC 20418

Ina Alterman
Board on Radioactive
Waste Management
GF456
2101 Constitution Ave.
Washington, DC 20418

Foreign Addresses

Studiecentrum Voor Kernenergie
Centre D'Energie Nucleaire
Attn: A. Bonne
SCK/CEN
Boeretang 200
B-2400 Mol, BELGIUM

Atomic Energy of Canada, Ltd. (3)
Whiteshell Research Estab.
Attn: B. Goodwin
M. Stevens
D. Wushke
Pinewa, Manitoba, CANADA ROE 1L0

Francois Chenevier, Director (2)
ANDRA
Route du Panorama Robert Schumann
B.P.38
92266 Fontenay-aux-Roses Cedex
FRANCE

Jean-Pierre Olivier
OECD Nuclear Energy Agency
Division of Radiation Protection
and Waste Management
38, Boulevard Suchet
75016 Paris, FRANCE

Claude Sombret
Centre D'Etudes Nucleaires
De La Vallee Rhone
CEN/VALRHO
S.D.H.A. BP 171
30205 Bagnols-Sur-Ceze, FRANCE

Bundesministerium fur Forschung und
Technologie
Postfach 200 706
5300 Bonn 2, GERMANY

Gesellschaft fur Reaktorsicherheit
(GRS) (2)
Attn: B. Baltes
W. Muller
Schwertnergasse 1
D-5000 Cologne, GERMANY

Bundesanstalt fur Geowissenschaften
und Rohstoffe
Attn: M. Langer
Postfach 510 153
3000 Hanover 51, GERMANY

Hahn-Meitner-Institut fur
Kernforschung
Attn: W. Lutze
Glienicke Strasse 100
100 Berlin 39, GERMANY

Institut fur Tieflagerung (2)
Attn: K. Kuhn
Theodor-Heuss-Strasse 4
D-3300 Braunschweig, GERMANY

Physikalisch-Technische Bundesanstalt
Attn: P. Brenneke
Postfach 3345
D-3300 Braunschweig, GERMANY

D.R. Knowles
British Nuclear Fuels, plc
Risley, Warrington, Cheshire WA3 6AS
1002607 UNITED KINGDOM

AEA Technology
Attn: J.H. Rees
D5W/29 Culham Laboratory
Abingdon, Oxfordshire OX14 3DB
UNITED KINGDOM

AEA Technology
Attn: W.R. Rodwell
O44/A31 Winfrith Technical Centre
Dorchester, Dorset DT2 8DH
UNITED KINGDOM

AEA Technology
Attn: J.E. Tinson
B4244 Harwell Laboratory
Didcot, Oxfordshire OX11 0RA
UNITED KINGDOM

Nationale Genossenschaft fur die
Lagerung Radioaktiver Abfalle (2)
Attn: S. Vomvoris
P. Zuidema
Hardstrasse 73
CH-5430 Wettingen, SWITZERLAND

Shingo Tashiro
Japan Atomic Energy Research
Institute
Tokai-Mura, Ibaraki-Ken
319-11 JAPAN

Netherlands Energy Research
Foundation ECN
Attn: L.H. Vons
3 Westerduinweg
PO Box 1
1755 ZG Petten, THE NETHERLANDS

Svensk Karnbransleforsorjning AB
Attn: F. Karlsson
Project KBS
Karnbranslesakerhet
Box 5864
10248 Stockholm, SWEDEN

Sandia Internal

1502	J.C. Cummings
6000	D.L. Hartley
6119	E.D. Gorham
6119	Staff (14)
6121	J.R. Tillerson
6121	Staff (7)
6300	D.E. Miller
6302	T.E. Blejwas, Acting
6303	W.D. Weart
6303	S.Y. Pickering
6341	A.L. Stevens
6341	Staff (6)
6341	WIPP Central Files (10)
6342	D.R. Anderson
6342	Staff (20)
6343	T.M. Schultheis
6343	Staff (2)
6345	R.C. Lincoln
6345	Staff (9)
6347	D.R. Schafer
7141	S.A. Landenberger (5)
7151	G.C. Claycomb
7613-2	Document Control (10) for DOE/OSTI
8523-2	Central Technical Files
9300	J.E. Powell